2012

Morphology controlled coating of catalytically active gold structures within flow-focused millifluidic reactor

Chelliah V. Navin
Louisiana State University and Agricultural and Mechanical College, navincv@yahoo.com

MORPHOLOGY CONTROLLED COATING OF CATALYTICALLY ACTIVE GOLD STRUCTURES WITHIN FLOW-FOCUSED MILLIFLUIDIC REACTOR

A Thesis

Submitted to the Graduate Faculty of the
Louisiana State University and
Agricultural and Mechanical College
in partial fulfillment of the
requirements for the degree of
Master of Science in
Biological and Agricultural Engineering

in

The Department of Biological and Agricultural Engineering

by
Chelliah V Navin
B.Tech., Karunya University, 2009
December 2012

ACKNOWLEDGMENTS

First and foremost I thank the Almighty God for guiding me as per his will.

I thank my parents Mr. C Vijayanathan and Mrs. Jamuna Vijayanathan and my little brother for their never ending love, prayers and guidance in all my endeavors.

I thank my Co-Advisors, Dr. Chandra S. Theegala and Dr. Challa S.S.R. Kumar, for the research opportunity and believing in me. Your guidance, kindness, wealth of knowledge and experience has helped my education further. I thank the Center for Atomic Level Catalyst Design, an Energy Frontier Research Center funded by the U.S. Department of Energy, Office of Science, Office of Basic Energy Sciences under Award Number DE-SC0001058 and the Board of Regents under grants award number LEQSF (2009-14)-EFRC-MATCH and LEDSF-EPS(2012)-OPT-IN-15 for funding this research.

Special thanks to Dr. Sai Krishna Katla for his help both as a committee member and as a friend for sharing his time and knowledge pertaining to this research. I thank Dr. James Spivey for his involvement in the committee for this thesis.

I thank the following people for their support and patience in helping with my studies: Dr. Steven G. Hall, Dr. Ronald Sheffield, Ms. Angela Singleton, Ms. Donna Elisar, Ms. Rhonda Shepard, Dr. Varshini Singh, Dr. Gudrun Lisa Bovenkamp, Dr. Kyungmin Ham, Dr. Dongmei Cao, faculty and staff of BAE, LSU and Center for Advances Microstructures and Devices (CAMD).

Finally, I thank my family and friends without whom my life would have been much harder. I thank all my fellow graduate and undergraduate friends and students for their help and assistance during my stay in LSU.

TABLE OF CONTENTS

LIST OF TABLES

LIST OF FIGURES

ABSTRACT

Synthesis of micro/nanomaterials within confined flow-based systems such as microfluidics has always been a promising research. However, the inability to scale up reagent volumes due to geometric constraints and pressure development within the channels at higher flow rates has limited their usage. In recent times, millifluidics has emerged as a useful technique where, apart from the synthesis, the *in situ* characterization of materials becomes easier. In this study, formation of morphology-controlled gold structures at different time intervals (*viz.* 1, 5, and 9 h) within a millifluidic chip reactor was investigated using gold chloride and dimercaptosuccinic acid (DMSA) as precursor reagents and sodium borohydride as the reducing agent. The structures formed were characterized using 3-D X-ray tomography, X-ray absorption near edge spectroscopy (XANES) and scanning electron microscopy (SEM). The X-ray tomography results show that the dimension of the gold structures vary with respect to their time of deposition within the channel. The gold structures formed at 1 h are 26 μm wide, 5 h are 55 μm wide and 9 h are 100 μm wide. However, the height of the gold structures remained relatively uniform and peaked at 27.5 μm for all the samples. The XANES results show that there are differences in the chemical nature and bonding of the structures before and after reduction with sodium borohydride. A linear combination fitting of the XANES spectra show 50% Au and 50% S with both Au-Au and Au-S bonding for the structures before reduction and 83% Au, 17% S predominantly Au-Au bonding after reduction with borohydride. The SEM of the gold structures show hemispherical shape for sample formed for 9 h, flower-shape for 5 h and polygonal-shape for the 1 h sample. The catalytic activity of these gold structures was also demonstrated through 4-nitrophenol and Ferricyanide conversion reactions. In both the

conversion reactions, the gold structures formed for 9 h flow time show better catalytic performance in terms of yield with 90.5% conversion for 4-nitrophenol and 85.5% conversion for Ferricyanide.

INTRODUCTION

1.1 Overview

Lab on a chip devices have become a promising topic of research as integrating and handling experiments in a small dimensional system is comfortable and easy to manipulate and scale up. Microfluidic devices emerged successful during the early 1980's to carry out laboratory experiments, where a better control over the reaction conditions like flow rate, temperature, concentration, mixing conditions, reaction rate, etc. is possible. Advantages of the using microfluidic devices include less volumes of reactant intake, quicker reaction response due to high surface to volume ratios, improved process control, portable analysis set-up, etc. The flow of reactant solutions in microfluidic devices is always laminar and is fed using pressure driven motion devices such as pumps (Whitesides and Stroock, 2001). The reactants with different chemical composition are adjacently pumped into the microfluidic devices which remain distinct until the point of mixing.

Assembly of microfluidic devices needs extensive fabrication techniques like photolithography and etching which are accurate but expensive. Sealing the channels in a microfluidic reactor is also extremely difficult and complicates the process for material characterization and analysis. Although, modern techniques like soft lithography, contact liquid photolithographic polymerization, etc. are used to fabricate microfluidic devices, the *in situ* characterization of materials in a microfluidic reactor is a tough task. Due to high capillary forces of the micro sized channels, the possibility of contamination of the reactants into undesirable surfaces is high. When the microfluidic devices are used continuously for an extended period of time, the reagents flow could cause channel blockage due to clogging (Haraldsson, 2005).

Due to advances in the millifluidic devices, *in situ* characterization of the particles and materials that are formed inside the millifluidic channels is easy. The internal channel dimensions in the millifluidic systems are many times larger. As a result, manipulation of reagents that are fed into these systems can be controlled and can withstand high pressures. Therefore, reactions involving higher flow rates can also be carried out with ease.

Unlike microfluidic systems, the techniques for millifluidic systems fabrication are easy and less expensive. Since, geometrical dimensions constrains are ruled out, the millifluidic systems are an efficient device for kinetic and chemical studies (Biswas *et al*., 2012). In a millifluidic system, as a result of higher flow rates and low pressure drop, shorter residence time can be achieved continuously without any clogging and blocking of the channels. Due to the reduced volume reactant feed, under controlled chemical and reaction conditions, the millifluidic systems allows efficiency in mixing-and-monodispersity in size of the particles formed..

The overall goal of this research is to study the morphology-controlled growth of gold structures within millifluidic reactor and demonstrate their catalytic activity. In previous studies, millifluidic devices were used in synthesis of catalytically active nanomaterials (Li *et al.*, 2012). Gold is selected as an appropriate choice because it has unique structure-dependent electronic and optical properties. Additionally, the resultant gold micro/nanostructures could be envisaged for several promising applications. Applying this technique, it is easier to synthesize similar atomically precise gold catalysts.

The morphology controlled formation of gold structures serves as a prototype to prove that synthesizing and characterization of any type of catalyst within the millifluidic channels is possible under controlled reaction and chemical conditions. Since it is possible to characterize the *in situ* formation of materials within the millifluidic reactor, the time-resolved growth of the

gold structures can be clearly studied at different flow rates. Factors like size, structure, distribution, thickness, layer, porosity of the gold structures formed in the reactor was observed using spectroscopic analysis, X-ray spectroscopy studies and kinetic calculations using two different catalytic reactions namely 4-nitrophenol reduction and Potassium hexacyanoferrate (III) reduction were carried out.

2. LITERATURE REVIEW

2.1. Catalysts

Catalysts play a crucial function in laboratory research and chemical industries. They are the substance which can control the rate of the reaction without being consumed. It is very important to select the correct catalyst for any reaction. Catalysts are mostly used in chemical, petroleum, pharmaceutical, biological industries. Use of inappropriate catalysts in industries could lead to undesirable circumstances. Therefore, for a reaction to take place efficiently by all means, appropriate catalysts have to be selected based on several factors which include size, shape, porosity, thickness, stability, mechanical strength, thermal characteristics, etc. These factors are based on understanding the structure and chemistry of the surface of the catalyst. The surface of the catalyst is where the reaction takes place.

In order to determine a catalyst for fundamental research, characterization of the catalyst is a must to investigate the active sites over its surfaces in molecular detail. Various scientific methods provide the composition, oxidation state of the catalyst. There are techniques when combined with high spatial resolution; the atomic level on the structure of the catalyst can be studied with ease. Synthesizing a catalyst which has a defined size and morphology with structural activity, particle size effects is a challenging task (Niemantsverdriet *et al.*, 1999). Most often heterogeneous catalysts are used for any reaction to take place to avoid expensive techniques to separate the catalyst from products. The properties of the catalyst vary substantially when used repeatedly, limiting its life span from second to years. Synthesizing a heterogeneous catalyst and its development has been always a trial and error experiments. (Campanati *et al*., 2003)

2.2. **Traditional catalyst preparation**

Catalysts can be differentiated into two types via Homogeneous and Heterogeneous. The first reported catalytic reaction was the oxidation of SO_2 to SO_3 using a homogeneous catalyst NO in 1750 (Farnetti, *et al.*). Traditionally, the techniques that were used to synthesize these two types of catalysts are precipitation, grafting, impregnation, vapor deposition, atomic layer deposition, etc. The important factor that has to be taken into account while preparing a catalyst traditionally is to develop a support which has a high surface area. Another important aspect for catalyst synthesis is to have a stable dispersion of the reactant which forms the catalyst. Briefly, catalyst preparation is classified into metallic (supported and unsupported) and non-metallic (supported and unsupported). Synthesizing a proper support with appropriate pore volume, pore size distribution and controlled surface area for supported metal catalysts has always been the field of research for several years. Deposition of non-metallic catalysts is easier onto the support materials to afford a high dispersion of the active component. Impregnation, gel precipitation and adsorption from solution are some of the techniques used for preparing supported non-metallic catalysts. Although X-ray and various spectroscopic techniques are applicable, due to not so broadly available selective chemisorption procedures, characterization of supported non-metallic catalysts is difficult than the supported metallic catalysts.

2.2.1. **Demerits**

Although catalysts help in controlling the speed and kinetics of the reaction; they also have certain demerits. After a certain catalyzed chemical reaction, it is necessary to separate the catalyst from the products and the remaining reactant solutions. Recovery of these catalysts when they are homogeneous with the products becomes extremely difficult. It takes a lot of process to

separate it from other products which is an expensive step. In order to remove a homogeneous catalyst, processes like distillation of reaction products, elimination of precipitating counter ions should be done to reuse the recovered catalyst. During these processes there are ample chances for the catalyst to lose its activity which may result in deactivation of the substance. A similar situation is encountered while using a heterogeneous catalyst too. Leaching of the heterogeneous catalyst during a reaction is one of a major disadvantage during its recovery.

As mentioned earlier, for a reaction to occur efficiently, selection of appropriate catalyst is necessary. Therefore, catalyst preparation should be monitored to get the correct morphology and structure. In a flask based chemical synthesis of a catalyst, there are chances of uneven mixing of reactant solutions during which the shape and size of the catalyst synthesized could vary. This disordered synthesis will lead to different morphology of the catalyst and could result in agglomeration where active sites over the catalyst could be masked by another catalyst. While using catalysts synthesized through traditional methods, due to undispersed reaction mixture, there are lot of chances for reduced chemical conversion.

2.3. Nanostructured and mesoporous materials

Nanomaterials have novel chemical, biological and physical characteristics. These materials can be used for catalysis, drug delivery, sensors, structural, electronic, photonic and various applications and fields. In recent times, nanotechnology has proved to be an efficient technique for preparing nano sized crystalline and porous materials which have unique properties. Due to their size, nanomaterials have high surface to volume ratio which can be characterized by their pore size and structures.

Nanomaterials are widely used in the catalytic research due to their versatile properties (Ying, 2006).

Synthesis of metal nanoparticles is done in two ways. (i) Bottom up method – where the primary building blocks are assembled to form nanostructures. Few examples for the bottom up method are nanosphere lithography, templating, chemical, electrochemical, sonochemical, thermal and photochemical reduction techniques. (ii) Top down method – where the large materials are cut down to nanoscale materials. Few examples of the top down methods are photolithography and electron beam lithography.

To prepare a nanocatalyst, control over the chemistry, structure and environment is important since these conditions affect the stability, selectivity and the activity of the catalyst. Traditional method by which nanocatalysts were prepared are thermal evaporation in vacuum, electron-beam lithography and pulsed laser deposition, buffer-layer assisted growth, chemical vapor deposition, gas condensation, ionized cluster beam deposition, electrochemical deposition methods, sol–gel or colloidal techniques, deposition–precipitation and impregnation methods, molecular cluster precursors, quantum electrodynamics induced electromagnetic radiation, etc. To control the growth of the nanocatalysts within a nanoreactor, suitable organic ligands are used to limit its morphology. Nanocatalysts are used in lot of applications which include Environmental remediation, noxious vapor control, Bio-particle sterilization, Renewable energy in the solar energy harvesting, hydrogen production, polymerization, etc. (Cuenya, 2010).

Mesoporous materials are catalytic substances having pore with diameters between 2 and 50 nanometers. Due to their surface area and large pore volume, mesoporous materials are used as an efficient heterogeneous catalyst. Mesoporous materials require surfactants as a template material for its synthesis.

2.3.1. Thermal evaporation in vacuum

It is a process where a hot source evaporates and condenses onto the substrate. The whole process is carried out in a vacuum chamber to avoid undesirable products formation *i.e.* in a evaporation chamber the heat sources vaporizes the reactant which travels in upper direction where there are lot of chances where it might react with the gaseous substances within the evaporation chamber to form oxides which might not be a desired product. Hence these unwanted vapors limit the quality of the vacuum process. Evaporation is commonly used in micro fabrication techniques for nanocatalyst preparation. Usually, the nanocatalyst prepared by thermal evaporation process is a thin film. The relative rate of the gaseous impurity is less and hence the purity of this thin film is higher at higher deposition rates. For synthesizing a nanocatalyst, electron beam is coupled to the thermal evaporation chamber to control the evaporation rate where the compound of interest to be formed can be deposited with known parameters.

However, there are certain demerits while using a thermal evaporation chamber for preparing nanocatalyst. The thickness of the nanofilm synthesized varies due to the geometry of the evaporation chamber. When the process is carried out under poor vacuum condition, there are chances where the deposition of the nanofilm becomes non uniform. ZnO nanobelts, MgO nanocubes, CdS, $CuInSe_2$, etc. are few thin nanofilms prepared using thermal evaporation process.

2.3.2. Electron beam lithography (EBL)

It is a process where a beam of electron is emitted in a patterned fashion over a film called resist covered over a surface. The purpose of using a resist is to create small structures

which can be subsequently transferred to the substrate material by etching. This process is used to create nanostructures. Usually, EBL is used to fabricate metal nanoparticles.

However, when using an electron beam lithographic techniques to prepare a nanomaterial, there are chances where the beam can drift which could lead to instability in the electron beam pattern. Au is the most fabricated nanomaterial using EBL.

2.3.3. Pulsed laser deposition

This process is similar to thermal evaporation process where the target material is vaporized when a high power pulsed laser beam hits it converting it to atoms, molecules, electrons and ions before depositing it onto hot substrate as a thin film. However, this process can also be carried out in the presence of oxygen, where the end products formed are oxides. iron, carbon, cobalt, silicon etc. are few metals which are used to synthesize nanofilms using pulsed layer deposition.

The presence of particulates makes this process a little complicated. The composition and thickness of the nanofilm depend on the deposition conditions. Also it is very difficult to scale up the nanofilms to large wafers.

2.3.4. Buffer-layer assisted growth (BLAG)

In this process, due to the low surface free energy properties, inert gas like xenon is used as a buffer to prevent the interaction between the atoms deposited and the weakly interactive substrate. Due to its overwhelming applications, BLAG method is used to prepare nanostructures which are otherwise difficult to prepare. BLAG is used to grow any materials on any substrates. gold, copper, rhodium, platinum, iron etc. are few nanometals that can be synthesized by BLAG.

On a whole, BLAG is a useful method to deposit clusters of any type, but there is a huge differences in the shape and size of the final particles formed at the end between the substrates studied.

2.3.5. Chemical vapor deposition (CVD)

It is a process where the raw material of the desired product to be formed is reacted with the substrate of interest. Most commonly, this technique is used in micro and nanofabrication where carbon nanotubes and carbon nanofibers are desired products.

In CVD, heat or plasma breaks the material of interest into reactive radicals which diffuse and absorb to the substrate within a quartz tube or a stainless steel container. A major disadvantage of this technique is that the growth of the particle formation is not easy to control.

2.3.6. Inert gas condensation

The material of interest is evaporated using a heated metal source to a chamber which is filled with low pressure inert gas. The metal vapor cools within this chamber by colliding with the inert gas atoms and nucleates homogeneously after super saturation. The particles thus formed are usually 1-100 nm. The particle size in this process can be controlled by varying the inert gas pressure. Decahedral and Icosahedral gold nanoparticles are generated using inert gas condensation process. Nanocrystalline materials such as PbF_2, Mn^{2+}-doped PbF_2, Sn-doped In_2O_3 (ITO), ZnO, Al_2O_3, Ag_2O, CdO, CuO, ZnSe:ZnO etc.,. Controlling the growth of the particles to retain the structure of the nano sized materials and preventing the agglomeration of the newly synthesized nanomaterials are some of the disadvantages in this process.

2.3.7. Ionized cluster beam deposition (ICB)

ICB is a process where materials are vaporized to form aggregates of atoms. These atoms are ionized by electron compact and accelerated by high potentials toward the substrate to form a film deposition. The acceleration of these ionizes atoms can be controlled by varying the voltage thereby controlling the film deposition of the metal over the substrate.

However, the film growth mechanism of the nanocrystalline structures by ionized cluster beam deposition is not fully understood (Perez *et. al.*, 1995). Fe, Ni, Co and other metal with magnetic properties are prepared using ICB.

2.3.8. Electrochemical deposition methods

It is a process where the metal ions present in a solution is accelerated towards a substrate under the influence of an electric field. This process is used commonly in synthesizing nanocrystallines, nanocomposites, nanofilms etc. by controlling the electrolysis parameters. Pulse current depositions, deployment of additives and surfactants and nanoparticles inclusion into deposits to form nanocomposites are few techniques used in electrochemical deposition.

Cobalt, nickel-cobalt, nickel-copper and zinc-nickel are few of the nanostructured materials prepared by electrochemical deposition technique. A possible disadvantage of using electrochemical deposition technique is contamination of the film from the solution. Particles with film, tubes and wire like structures with nanosized dimensions are deposited easily by electrochemical deposition technique (Podlaha *et. al.*, 2006).

2.3.9. Sol–gel or colloidal techniques

Metal chlorides and alkoxides acts as the precursor fluids which are dispersed into the host fluid to form a colloidal solution. This solution is deposited over a substrate to form particles and films of nanosize. Iron oxide nanoparticles, CdS, TiO_2, SiO_2 and ZrO_2 are few nanoparticles prepared using this method. The sensitivity of the atmospheric condition is a major drawback using sol-gel or colloidal technique for nanomaterial preparation. The chances of contamination due to toxicity from the solvent system are quite high which could reduce the quality of the nanomaterial prepared.

2.3.10. Deposition–precipitation and impregnation methods

The catalysts used in the industries currently are formed primarily by deposition-precipitation and impregnation methods. The metal salts are precipitated from the solution on the substrate material and further dried to small nanoparticles by thermal methods. The size, dispersity and the shape of the nanoparticle is controlled by varying the pH of the metal salt solution and the support on which the nanoparticle is synthesized. Based on the nature of the metal salts, the substrate is selected according to its acidic and basic feature to facilitate the salt precipitation and deposition. This variation helps in better particle size control and includes subsurface metal inclusion, thus making the characterization more difficult.

2.3.11. Colloidal synthetic preparation of nanoparticles

To prepare a nanomaterial through colloidal synthesis, thermal decomposition it used more often to prepare particles of smaller dimensions. The use of surfactants in the colloidal

synthesis helps in direct particle growth and restricts the particle size and stabilizes the colloidal suspensions to prevent aggregation and precipitation. Surfactants are also termed as ligands which bind to the particles mainly due to the surface interacting functional group and possess a solvent soluble chain for easy solubility into the solution.

2.3.12. Packed bed reactors

Packed bed reactors with solid catalyst particles and are used primarily in heterogeneous phase reactions. Advantages of packed bed reactors are high conversion per unit mass of the catalyst, low operating cost and continuous operation. However, existence of undesired thermal gradients at some points, poor temperature control, and chances of developing back pressure at higher flow rates, channeling and difficulty in cleaning and maintaining the reactor are few disadvantages that are encountered.

2.4. Formation mechanism of monodisperse nanoparticles

A reactant has to undergo three stages to form a particle *i.e.* super-saturation, nucleation and growth. The monomers start to form in stage I where there is no particle nucleation until it reaches the saturation point. After reaching this critical point, the monomers start to nucleate at stage II resulting in decreased particle concentration. In stage III, the nucleation of the new particles ceases due to the decrease in the concentration of the monomers below the critical saturation point. At this point, the particle growth is initiated which is obtained due to the short nucleation period and slow growth kinetics to control the size of the particle.

2.5. Strategies for controlling size and shape of nanoparticles

Surfactants play a significant role in controlling the size of the nanoparticle. Using stronger and diluted surfactants may result in small and large sized nanoparticles respectively. Other method to control the size of the nanoparticle is to regulate the metal precursor concentration to have a better control over the nucleation and growth of the nanoparticles. The size and the structure of the nanoparticle are important for any chemical reaction. However, when synthesizing a nanoparticle by colloidal chemistry method, the internal structure of the nanoparticle varies for any given concentration. This variation influences the morphology of the nanoparticles synthesized. Although nanoparticles synthesized by the above mentioned methods give a promising data and success, more work is needed to remove the encapsulating ligands completely from them after synthesis. Such drawbacks stress the need for material characterization before conducting any experiments to get the desired results (An *et al*., 2012)).

2.6. Lab on a chip devices

2.6.1. Microfluidic device

To overcome the demerits of the techniques described above for nanocatalyst preparation, the application of microfluidics came into existence in the early 1990's. Microfluidic technology is a subset of lab on a chip device which is used in versatile practical applications. Microfluidic devices are few millimeters to few centimeters in size.

Microfluidic devices are used to synthesize micro/nanoparticles with a control over their size, structure and composition. Nanosized materials are prepared in smaller volumes using the traditional batch techniques where the reproducibility of the size, composition, quality of the

nanoparticles synthesized differs when repeated under the same practical conditions. The biggest drawback when synthesizing a nanoparticle in a traditional batch reactor is that, the optimization of these materials becomes extremely difficult. Whereas, when a microfluidic device is used where the reaction conditions are continuous, there is an advantage of coupling instruments which controls the flow of the reactants and enhances the efficiency of the whole set up. In a traditional batch nanoparticle synthesis, scaling up of the reaction conditions is difficult. Other advantages of using microfluidic devices are low fluid volumes, good process control, low fabrication costs, quicker analysis, compact, safe and reproducible results.

A microfluidic device is a lab on a chip device constructed to perform a chemical reaction which is designed in such a way to maximize the efficiency of the reaction conditions. The huge aspect of performing a reaction in a microfluidic reactor is that, the reaction conditions can be controlled desirably according to flow rate, concentration, pressure etc. Early microfluidic devices had stainless steel, polymer tubing to provide reactant flow into the reactor. However, with repeated experiments, silica tubing is being used nowadays to achieve proper mixing and preparing hydrodynamic micro and nanostructures. These capillary tubing are inflexible to integrate equipment for monitoring the state of the reaction. Whereas the microfluidic reactor helps in precise manipulation of the fluids and reagents flowed within the channels for better mixing.

2.6.2. Fabrication of microfluidic reactor

Fabrication of microfluidic reactor is done based on constrains of the material used in the synthesis. Polydimethyl siloxane (PDMS) is the most commonly used polymer in microfluidic reactor fabrication. The microfluidic reactor can be fabricated easily by photolithography

technique coupled with negative photoresist at a low cost. The major drawback in a microfluidic reactor fabrication is that they have minimal operating pressure and lack chemical compatibility because most solvents disrupt the bonding of PDMS to the glass. To avoid this problem, surface modification of the PDMS micro reactors were designed. Fluoropolymer and glass, SU-8-PEEK microfluidic reactors were designed to undergo reactions at elevated temperatures. In contrast, metal microfluidic reactors were also fabricated by electrofoaming, electro-discharge machining and laser ablation. Ceramic microreactors, glass/glass micro reactors, PVC, silicon-pyrex are some of the materials used for micro fabrication. The microfluidic reactors fabricated using silicon materials prove to be an efficient lab on a chip device under high temperature conditions.

2.7. Preparation of micro and nanostructured materials within the microfluidic reactor

2.7.1. Metal nanoparticles

Many inorganic and organic nanoparticles have been synthesized in a continuous manner with more control over the particle size distribution, shape and quality of the nanomaterial. Metal nanoparticles, oxide nanoparticles, semiconductor nanoparticles, QD core shell structured micro and nanostructures are few types of nanomaterials synthesized through microfluidic reactor.

Most often reducing salts are used in synthesizing metal nanoparticles. Sodium borohydride, lithium hydrotriethyl borate, 3-(N,Ndimethyldodecylammonia) propane sulfonate, sodium citrate are used as the reducing salts. Microreactor fabricated sing glass capillaries, PDMS-glass are used to synthesize metal nanoparticles under room temperature. There is a lot of probability of the micro and the nano structures to agglomerate within the channels of the microfluidic reactor. Therefore, using surfactants and ligands helps in preventing the cluster formation of the structures and helps in deposition of the structures to the channel walls.

The synthesis of micro and nanostructures within the microfluidic reactor is done in two ways. The first method is where the reactant solutions are fed into the microreactor followed by the addition of the second reactant into the microfluidic reactor. To reduce the risk of agglomeration, ligands and surfactants are passed through the microreactor in the final step. This is a single step synthesis where there is a continuous addition of the reagent and easy to implement. The disadvantage of using this approach toward micro and nanomaterial synthesis is that the reactants within the microfluidic reactor has large residence time distribution due to the continuous single phase reaction condition where there is a huge possibility of clogging of the reactants within the channels which could result in loss of optical and absorption studies. The second approach toward the synthesis of micro and nano sized materials within the microfluidic reactor is that the reaction solutions are fed simultaneously within the microfluidic reactor through separate inlets. These reactants mix together within the microfluidic reactor where the nucleation and the growth of the nanostructures take place. This method is called the droplet-based approach. The second approach for the synthesis of the micro and the nanostructured materials is preferred because of its short residence time distribution and less chances of clogging (Marre and Jensen, 2010).

2.7.2. Oxide nanoparticles

Apart from the metal nanoparticles, several oxides nanomaterials can also be synthesized within a microfluidic reactor. As of now, preparing an oxide nanoparticle has been carried out only in a room temperature conditions. To prepare an oxide nanoparticle, synthesizing the nanomaterial without control over its shape and size has been done so far within the microreactor. To prevent the clogging of the nanomaterials within the microreactor, 3D injection

is carried out coaxially through the capillary tubing. This method proved that the solutions flow in the center path within the microreactor channels without touching the channel walls. The other method is that the reactants are brought together within the microfluidic reactor by the effect of electrocoalescence, where the two reactants enter the reaction channels coupled with electrodes, which forced the reactant solutions to fuse each other due to current. This method is much faster and there is absolutely no contact between the nanoparticles synthesized within the microflulidic reactor to the microfluidic reactor walls. Narrow size distribution is achieved for the nanoparticles synthesized within the microreactor when an inert second phase is created along with the segmented flow reaction system where there will be no interaction between the individual droplets since the dispersion effects are eliminated. In the continuous phase reaction method, there is a high probability that the reactants can be interchanged which could lead to broader size distribution of the nanomaterials. So, to ensure a narrow size distribution of the nanomaterials within the microfluidic reactor, segments flow method is followed and gases are used as the inert material because there is a big advantage of removing or adding it easily. Core shell structures can be synthesized within the microreactor when the reacting medium interacts with the walls of the microreactor by adding the reagents to the reacting phase. However, there is broadening in the size distribution when the reacting medium interacts with the walls of the microreactor. More complex structures can be achieved through microfluidic reactor through sol-gel chemistry technique.

2.7.3. Crystalline semiconductor nanoparticles

Other than metal and oxide nanomaterials, quantum dots and semiconductor nanomaterials have also been synthesized using the microfluidic reactor where low reagent

consumptions is enough to optimize the enhancement of the quantum dot and semiconductor nanomaterials. Droplet electrocoalescence, segmentation of the reactants in contrast to the continuous approach are few options to prepare quantum dots and semiconductor nanomaterials for narrow particle size distribution. A huge drawback of using microfluidic reactor at elevate temperatures is that the solvents, ligand and the precursors remain liquid for the entire reaction. Single phase laminar synthesis approach is preferred for manufacturing microchips since it is flexible in space and design and easy for online characterization. However, few limitations are observed in the single phase laminar synthesis approach, where there is broadening of the size distribution of the nanomaterials due to high viscosity, slow mixing and long residence time distribution. Few other methods to achieve narrow size distribution are by preparing the nanoparticles by flow segmentation method where the reactants have improved mixing and narrow size distribution. Other method is cross flow focusing where the size of the reactants is brought down to few microns. Also when the supercritical fluids are used instead of the high boiling point viscous solvents systems, a narrow size distribution of the micro and nano materials can be achieved.

2.7.4. Heterogeneous and hybrid micro and nanoreactors

Heterogeneous and hybrid micro and nanostructures are synthesized by continuously adding the reagents into the microreactor where the solutions decompose quickly and thus creating nucleation and deposition of the microreactor walls. A region of critical concentration is achieved by feeding the coating solution into the microreactor to create the nucleation of the nanomaterial. There is no possibility of nucleation due to continuous feeding of the reactants where the microreactor channels have a low concentration levels. To ensure equal flow rates at

each point, the microreactors were designed to have side channels which are shallow. This model helps in flexibility in synthesizing the micro and nano structures with more control over the concentration, size and morphology. To improve the efficiency of the micro and nano materials, surface modification of these materials is done to have specific properties. Organic and inorganic hybrid micro and nanoparticles can be achieved by solvent evaporation technique where the core shell is synthesized in PLGA microcapsules. The particle morphology can be controlled by masking the design of the particle structure. The magnetic properties of the micro and nanoparticles can be assembled correspondingly when they are induced into a magnetic field.

2.7.5. Nanoparticles shapes and sizes

The shape and the size of a nanoparticle (NP) play a vital role in every chemical reaction. By having the correct particle shape and size, all the chemical reactions can be easily controlled. Usually a nanoparticle's size varies from 1-100 nm. The shape of a NP can be controlled by a capping agent, fluorescent light to convert the surfactant stabilized over the NP. More research is carried out at present on various shapes of NP like nanodisks, nanoplates, etc. with respective to its optical and physical properties. NP synthesized within polymeric materials can be prevented from oxidation and helps in long stability of these materials. A lot of research has been done to incorporate various shapes of NP in polymer composites. The initial step is the connection of the metal particles across the sample called the percolation threshold. When the concentration of the filler particles is increased to this threshold, clusters is formed which starts to increase in size. Developments are made in nanotechnology using the polymer matrices to create various shapes of NP.

2.8. Nanoparticles synthesized within microfluidic reactor

There are various types of nanoparticles synthesized using a microfluidic reactor. These types include, metal nanoparticles, oxide nanoparticles, quantum dots, heterogeneous nanoparticles, hybrid microparticles and other nanocrystalline materials. The synthesis of these nanoparticle and microparticles vary accordingly with respective to the temperature and the type of microfluidic reactor used (Marre and Jensen, 2010).

2.8.1. Metal nanoparticles

Metal	Microreactor
Copper Nanoparticles	SU-8-PEEK
Palladium Nanoparticles	SU-8-PEEK, Glass Capillary
Silver Nanorods	PVC and PEEK Tubing
Silver Nanoparticles	Silicon – Pyrex

2.8.2. Quantum dots

Metal	Microreactor
CdS	PDMS-Glass
CdSe	Glass-Glass
CdSe	Silica capillary
CdSe	Silicon-Pyrex
InP	Silica capillary
Si_3N_4	Ceramic

2.8.3. Oxide nanoparticles

Metal	Microreactor
Fe_3O_4	PDMS-Glass
ɤ- Fe_3O_4	PDMS-Glass + Capillary injection
α-FeOOH	PDMS-Glass + Capillary injection
SiO_2 Nanoparticles	PDMS-Glass
Silicalite	SS Capillary
SiO_2 microspheres	PDMS-Glass
SiO_2 microspheres and slugs	Silica capillary
TiO_2 hollowspheres and nanorods	PDMS-Glass

2.8.4. Heterogeneous nanoparticles and hybrid microparticles

Metal	Microreactor
CdSe@ZnS	Silica Capillary, Silcon-Pyrex
CdSe@ZnSe	Silicon–Pyrex
SiO_2@TiO_2	PDMS–Glass
ɤ-Fe_2O_3@SiO_2	Silica capillary + PDMS–Glass
[CdSe@ZnS] in PLGA microgels and microcapsules	Silica capillary x+ PDMS-PDMS
ɤ -Fe_2O_3 in micro hydrogels	PDMS–Glass + aluminium reflectors
ɤ -Fe_2O_3 or QDs in PNIPAm micro capsules	Capillary-based Microsystem
Superparamagnetic Janus particles	PDMS–Glass + aluminium reflectors

2.8.5. Catalytically active gold nanostructures within microreactors

Metal	Microreactor	Reactant
Gold Nanoparticles	Glass-glass	HAuCl4 + $NaBH_4$ + dodecanethiol
Gold Nanoparticles	PDMS-glass	HAuCl4 + Trisodium citrate
Gold Nanoparticles	Silicon-pyrex	HAuCl4 + Ascorbic acid + PVP
		HAuCl4 + Ascorbic acid + Fe(II) + PVOH + Na2SiO3
Gold Nanorods	PVC and PEEK Tubing	Seeds + HAuCl4 + $NaBH_4$ + CTAB
Gold Nanorods and nanoclusters	PDMS-Glass	(Au seeds) + HAuCl4 + Ascorbic Acid + CTAB

2.9. Millifluidic reactor

Due to its overwhelming advantages and applications, millifluidic reactor is used as a substitute for thermodynamically metastable systems for continuous flow microfluidic reactor for synthesizing micro and nanostructured materials. Advantage of using a millifluidic reactor is to produce particles with narrow size distribution with polydispersity. Many experiments were done with the microfluidic reactor with rapid continuous synthesis of monodisperse paricles. Although the microfluidic reactors have geometrical constrains, they are used to prepare non-spherical particles with control over its morphology and size. The millifluidic reactor offers good scope in controlling the size and the shape of the structures synthesized within it in a continuous flow method. It offers various features which is impossible to achieve in batch and microfluidic reactors. The advantage of using a millifluidic reactor is that, it is easy to generate highly monodisperse liquids and easy to manipulate the reagents online. The collisions between the

droplets within the millifluidic reactor are suppressed and as a result the effect of coalescence is not needed to be stabilized. Due to its higher flow rates, particle production with sizes from micro to nanoscale, monodispersity, design and low cost fabrication, millifluidic reactor is a best method to prepare micro and nanostructured particles.

Millifluidic reactor can be used to achieve droplet based kinetic measurements instead of microfluidic reactor. The setup of the millifluidic reactor is fast and easy to control. The residence time of the reactant within the millifluidic reactor can be controlled from short to longest time without altering properties of the channels. When there is a need for two fluids to be taken within the millifluidic reactor, it offers possibilities to overcome the gravity effects without breaking the symmetry of the flow of the reactants.

2.9.1. Millifluidic reactor fabrication

The modern millifluidic reactors are fabricated as chips using polyester terephthalate and acrylic pressure sensitive adhesive. This chip demonstrates that the larger molecules diffuse slowly *i.e.* there is a molecular weight dependent diffusion between two streams flowing side by side within a channel. These reactors are designed to carry out chemical conversions at ambient temperature. However, certain millifluidic reactors are fabricated to carry out chemical reactions at elevated temperatures. These reactors are made with polyetheimide commonly known as ULTEM and silicone pressure sensitive adhesive. These reactors can withstand temperatures up to 170 °C.

2.10. Gold catalysts

Due to its intrinsic value and properties, gold has always been considered as a novel metal of all the elements. Catalytically active gold nanoparticles and nanorods were earlier synthesized under various reaction conditions in the microfluidic reactor. glass-glass, PDMS-glass, PVC and PEEK tubing, silicon-Pyrex, PDMS-glass types of microfluidic reactors were earlier used for gold catalyst preparation (Marre and Jensen, 2010). Gold prepared using the microfluidic reactors offered less scope toward its characterization in order to study its morphology and structural chemistry. In recent times, this disadvantage is overcome by synthesizing catalytically active gold micro and nano structures in a millifluidic platform. Gold catalyst prepared in this method offered greater scope in spectroscopic probing and other techniques to study its properties. A compared study between millifluidics-based synthesis and traditional flask based synthesis of gold micro/nanostructures shows that size and morphology of the gold can be controlled by varying the flow rates using the millifluidic systems. Although a similar reaction condition is encountered in microfluidic reactor where the size and morphology of the gold can be controlled by varying the flow rate of the catalyst reagents, the potential advantage in a millifluidic systems is that the fluid volumes is many times larger which offers ease of flow rate control and ability to manipulate the reagents controlling the reagents (Weibel and Whitesides, 2006).

To sum up, gold catalysts can be prepared using millifluidic systems which offer greater scope in characterization and can be employed as a tool for time resolved kinetic studies and spectroscopic methods.

3. MATERIALS AND METHODOLOGY

3.1. Materials

All the chemicals Chloroauric acid ($HAuCl_4$, 99.9%), Dimercaptosuccinic acid (DMSA, 98%), Sodium hydroxide (NaOH, 99.9% pellets), 4-nitrophenol (99%), 4-aminophenol (99% HPLC grade), Sodium borohydride ($NaBH_4$, 98%), Potassium hexacyanoferrate (III) ($K_3Fe(CN)_6$, 99%), Hydroxymethyl furfural (HMF, 99%), Furandicarboxylic acid (FDCA, 97%) Levulinic Acid (LV, 98%), Formic acid (FA, 95%), Succinnic acid (SA, 99% reagent plus), Lipoic acid (α - LA, 99%) and Silver nitrate (AgNO3, 99%) were provided by Sigma Aldrich. The millifluidic reactor made of polyester terephthalate polymer channels with channel dimensions of 2 mm (W) x 0.15 mm (H) x 220 mm (L) and ULTEM (polyetherimide), manifolds to connect the pumps and the chip, tubing were purchased from Microplumbers Microsciences LLC. High precision, fully automated, pulsation free syringe pumps to flow the liquids within the chip were purchased from Cetoni Automation and Microsystems, GmbH. The water used throughout this study was Nanopure water (18.2 MΩ-cm).

3.2. Reagent preparation

3.2.1. Catalyst reagents

Standard solution of gold chloride (10 mM) was prepared by dissolving 118.2 mg of HAuCl4 (Aldrich, 99.9%) in 30 ml of Nanopure water. Standard solution (20 mM) of dimethyl succinic acid (DMSA, Aldrich, 98%) was prepared by dissolving 109.2 mg of DMSA in 30 ml of Nanopure water. Standard solution (10 mM) of sodium borohydride ($NaBH_4$, Aldrich, 98%) was prepared by dissolving 11.34 mg of $NaBH_4$ in 30 ml of Nanopure water.

3.2.2. Reagents for kinetic calculations

3.2.2.1. Reagents for 4-nitrophenol reduction

Standard solution of 4-nitrophenol ($9*10^{-2}$ mM) was prepared by dissolving 1.25 mg of 4-NP in 100 ml of nanopure water. Standard solution of sodium borohydride (0.65 M) was prepared by dissolving 2.45 grams of $NaBH_4$ in 100 ml of nanopure water.

3.2.2.2. Reagents for Potassium hexacyanoferrate reduction

Standard solution of potassium hexacyanoferrate ($8.33*10^{-4}$ M) was prepared by dissolving 2.74 mg of $K_3Fe(CN)_6$ in 10 ml nanopure water. Standard solution of sodium borohydride (0.01 M) was prepared by dissolving 3.78 mg of $NaBH_4$ in 10 ml of nanopure water.

3.3. Millifluidic reactor setup

The reactor has two identical flow paths with channel dimensions of 2 mm (W) x 0.15 mm (H) x 220 mm (L). The channel in the millifluidic reactor has two inputs and a single output which connects them to the manifold. A fully-automated pulsation free syringe pumps to flow the liquids within the chip was programmed to dispense the reagent solutions through the chip at the required amounts and flow-speeds through the computer operated software.

3.4. Method for gold catalyst deposition

10 ml each of the gold chloride (10 mM) and DMSA (20 mM) solutions were taken into two separate syringes and were flown within the chip with a uniform flow-rate of 1 ml/h at different time intervals (*i.e.* 1, 3, 5, 7 and 9 h) for several experiments (Figure 3.1 1). The mixing of the precursors resulted in the formation of gold sulfide ($Au_xS_y^-$) structures, which were then

reduced with 10 mM $NaBH_4$ by washing them~~it~~ in the $NaBH_4$ solution for 15 min at 5 ml/h flow-rate (Figure 3.1-2). The chip was finally washed with Nanopure water for 30 min at the same flow-rate before performing the catalysis experiments (Figure 3.1-3).

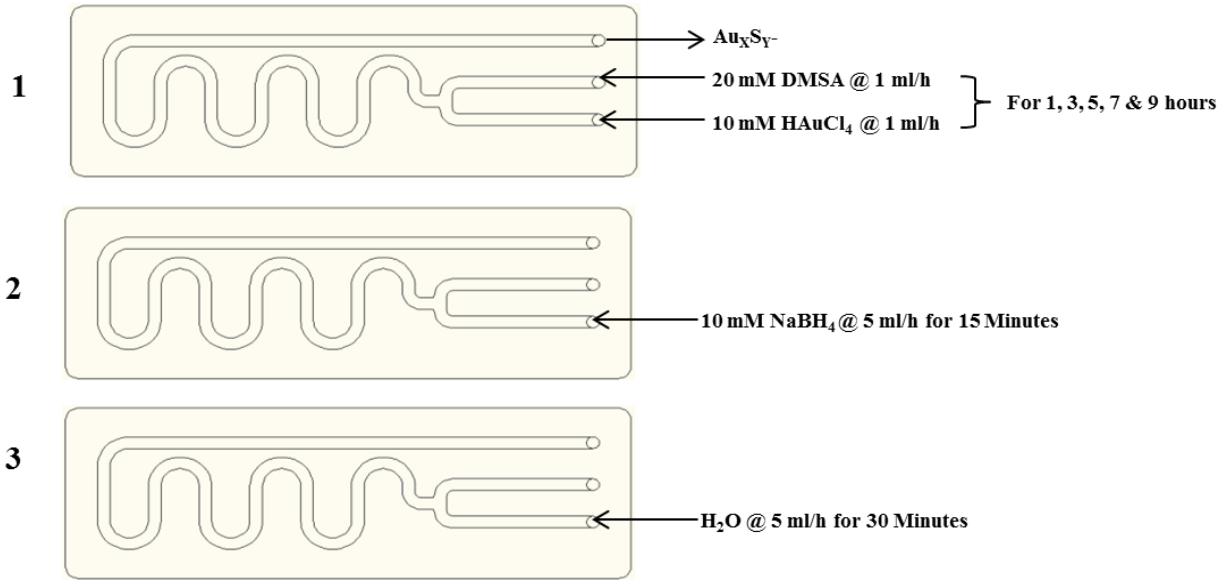

Figure 3.1: Pictorial representation of the synthesis scheme for gold structures formation within the millifluidic reactor

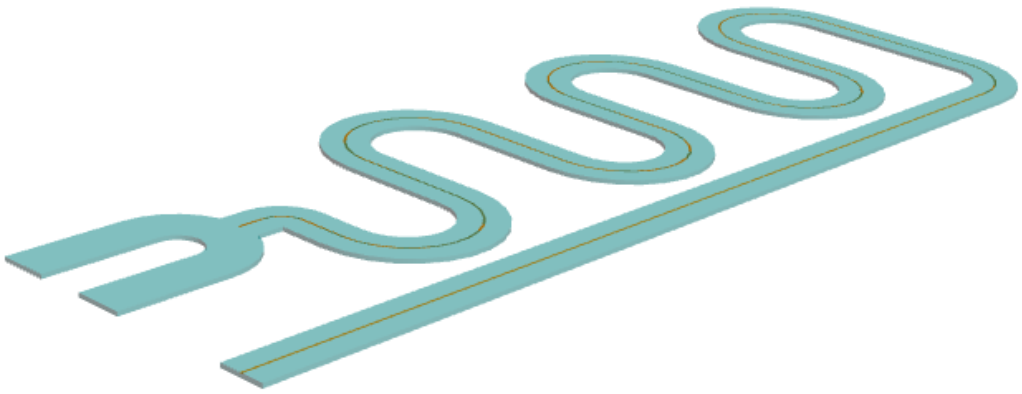

Figure 3.2: 3-D view of the millifluidic reactor channels after gold structures formation

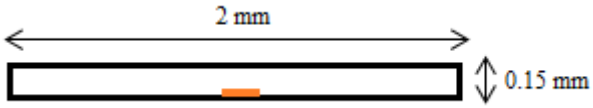

Figure 3.3: Cross sectional representation of gold structures formed with respect to the channel dimensions

3.5. Methods for characterization of gold nanoparticles

3.5.1. Scanning electron microscopy

Hitachi S-4500II cold field emission scanning electron microscope, with EDS detector, was used in this study to investigate the surface morphology of gold structures formed within the millifluidic channels. This SEM was equipped with large stage with motion ranges of 360˚ continuous rotation, -5˚ to 45˚ tilt, 0 to 100 mm in X, 0 to 50 mm in Y and 3 to 28 mm in Z direction, and can be used to image features at magnification from 20x to 500,000x, with resolution of 1.5 nm (at 15 kV accelerating voltage and working distance of 4 mm) or 4.0 nm (at 1 kV accelerating voltage and working distance of 3 mm).

3.5.2. 3-D X-ray tomography

High resolution X-ray tomography images were collected at Louisiana State University, Center for the Advanced Microstructures and Devices tomography beamline at 15keV monochromatic X-ray energy. Transmitted X-rays through the samples were converted to visible light with a synthetic garnet (Ce:YAG) scintillator and scintillator was imaged with a 5.4 X microscope objective focused onto a 16 bit CCD camera (Princeton Instrument PIXIS2KB

2048 x 512 pixels, each 13.5 µm x 13.5 µm), yielding an effective spatial resolution 2.5 µm . The sample was cut into a piece fitted in a field of view and mounted with clay atop the tomography sample rotation stage. Reconstructions of 766 images from 0° to 179.5° by 0.5° angle increment and double imaging with 10 pixels apart were performed using a MatLab program based on filtered back projection and double correlated sampling to reduce the ring artifacts.

3.5.3. X-ray absorption near edge spectroscopy (XANES)

The XANES experiments were carried out at the WDCM beamline of the synchrotron radiation source at Center for Advanced Microstructures and Devices (CAMD), Baton Rouge, USA, with an energy of 1.3 GeV using Ge (422) crystals for the Double Crystal Monochromator (DCM). For calibration, the energy of the Au-L_3 edge was set to 11919 eV using the first maximum of the first derivative of the metal foil spectrum. XANES spectra were measured with 3 eV equidistant energy steps in the pre-edge region of 11750 eV to 11900 eV, with 0.7 eV in the edge region of 11900 eV to 11200 eV and with 1.0 eV in the post-edge region of 12000 eV to 12400 eV. Data were normalized using a first-order spline for pre-and post-edge regions and analyzed using the ATHENA program of the IFFEFIT package.

3.5.4. UV-Visible spectroscopy

Optical absorbance of the catalysis samples were recorded using Shimadzu, UV-3600 spectrophotometer. 3 ml of sample was collected for each catalytic run and introduced into 10 mm Quartz cuvette and the absorbance was measured from 200 nm to 500 nm.

3.6. Catalysis reactions

3.6.1. 4-nitrophenol reduction

15 ml of 9 X 10^{-2} mM solution of 4-nitrophenol was mixed with 3.3 ml of 0.65 M $NaBH_4$ solution to form phenolate ion. This resultant solution was passed through the as-prepared gold structures deposited chip at different flow rates (5, 20, 40 and 60 ml/h) and the products collected were analyzed using UV-Vis spectrophotometer.

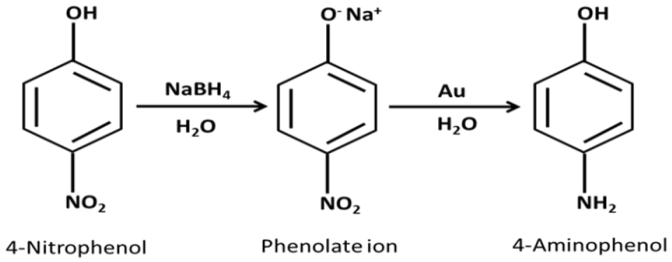

Figure 3.2: Conversion of 4-nitrophenol to 4-aminophenol

3.6.2. Potassium hexacyanoferrate (III) reduction

5 ml of 8.33 X 10^{-4} M hexacyanoferrate (III) was mixed with 1 ml of 1 X 10^{-2} M $NaBH_4$ solution and the resultant solution was passed through the chips at the different flow-rates (5, 20, 40 and 60 ml/h) and the products collected were analysed using UV-Vis spectrophotometer.

$$BH_4^- + 8\,[Fe(CN)_6]^{3-} + 3H_2O \xrightarrow{Au} H_2BO_3^- + 8[Fe(CN)_6]^{4-} + 8H^+$$

Figure 3.3: Conversion of ferricyanide to Ferrocyanide

3.6.3. Kinetic study for rate of the reaction

The kinetic activity was determined by measuring the products collected at different flow rates (5, 20, 40 and 60 ml/h) after the reduction reaction of 4-nitrophenol and Potassium hexacyanoferrate reactions with the gold deposited within the millifluidic chip. The reaction rates were calculated by obtaining the absorption peak values from the UV-Vis spectrum.

4. PREPARATION AND CHARACTERIZATION OF GOLD STRUCTURES WITHIN MILLIFLUIDIC REACTOR

4.1 Results and discussion

4.1.1 Morphology of gold structures within millifluidic reactor

Catalytically active gold (Au) structures within the millifluidic reactor were prepared by controlling the flow of $HAuCl_4$ and DMSA through the millifluidic channel at 1 ml/h for various time intervals (1, 3, 5, 7 and 9 h). These reagents mix together within the millifluidic reactor to form yellow colored gold sulfide ($Au_xS_y^-$) having an Au/S ratio close to 2 with Au(I) oxidation state (Figure 4.1) which was confirmed using XANES (Figure 4.11). This gold in oxidation state (I) was further reduced to Au^0 by treating the $Au_xS_y^-$ with $NaBH_4$ by controlling its flow at 5 ml/h for 15 minutes within the millifluidic reactor. The reduced gold was then washed with nanopure water at 5 ml/h for 30 minutes (Figure 4.2).

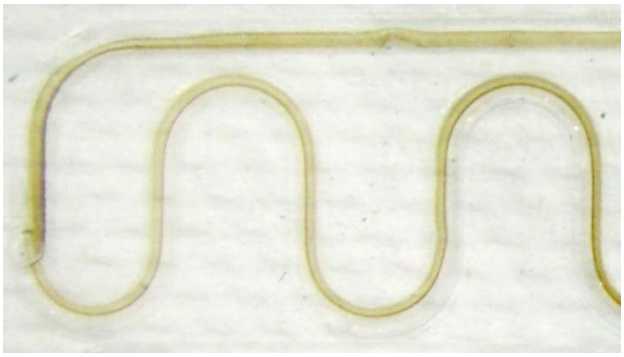

Figure 4.1: Gold in Oxidation state I

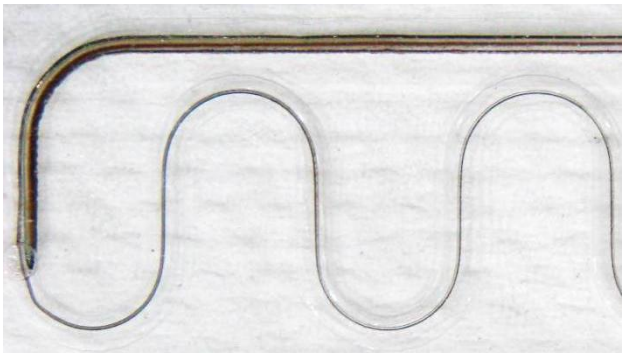

Figure 4.2: Reduced gold

The black thick line within the millifluidic channel from Figure 2 was observed under the scanning electron microscopic analysis at specific points for analyzing the structural morphology of the reduced gold structures deposited at 1 ml/h for time intervals 1, 3, 5, 7 and 9 hours.

Figure 3 shows the low-magnification SEM image of reduced gold structures formed after 9 h deposition of $Au_xS_y^-$ followed by 15 min reduction by $NaBH_4$. The image shows the formation of monodisperse gold microspherical structures. A closer view of the same (Inset of Figure 4.3) shows the microstructures to be hemispherical in shape.

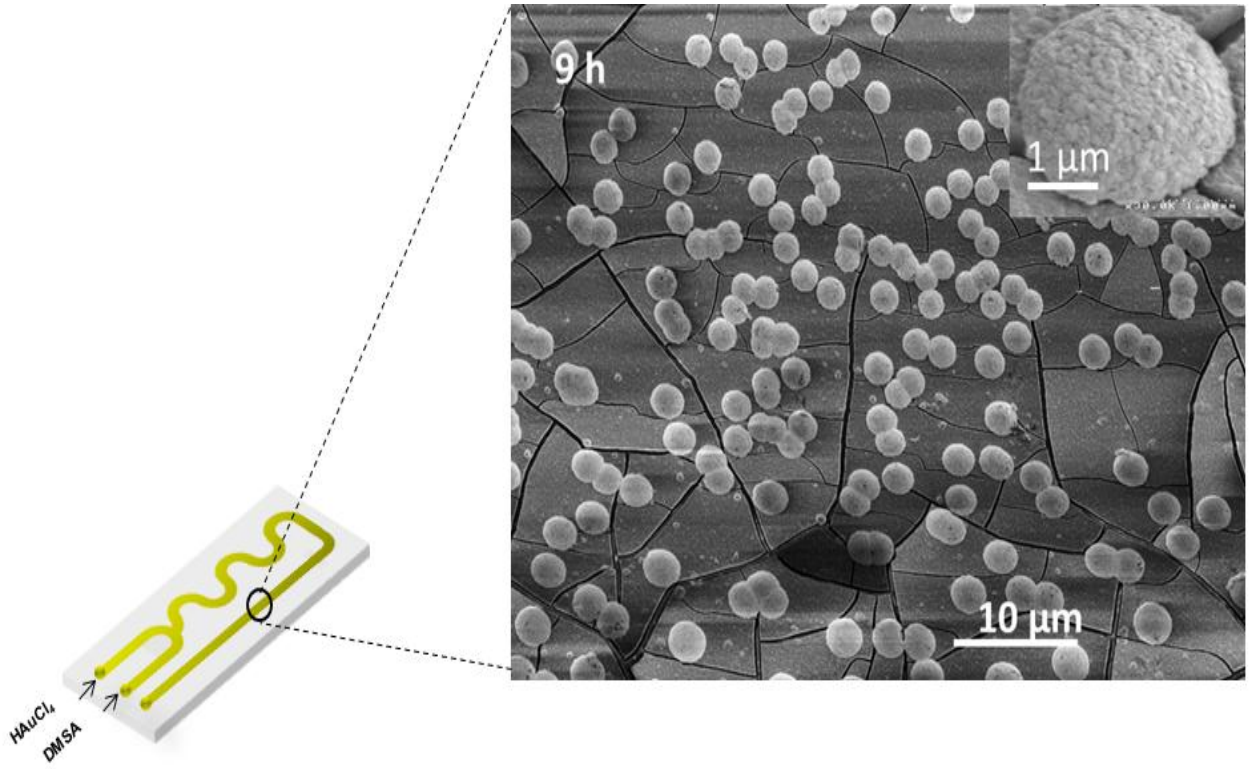

Figure 4.3: Gold structures formed at 1 ml/h flow rate for 9 h flow time

EDAX elemental analysis of these structures confirms that they contain both gold and sulphur from the DMSA after the reduction process (Figure 4.4)

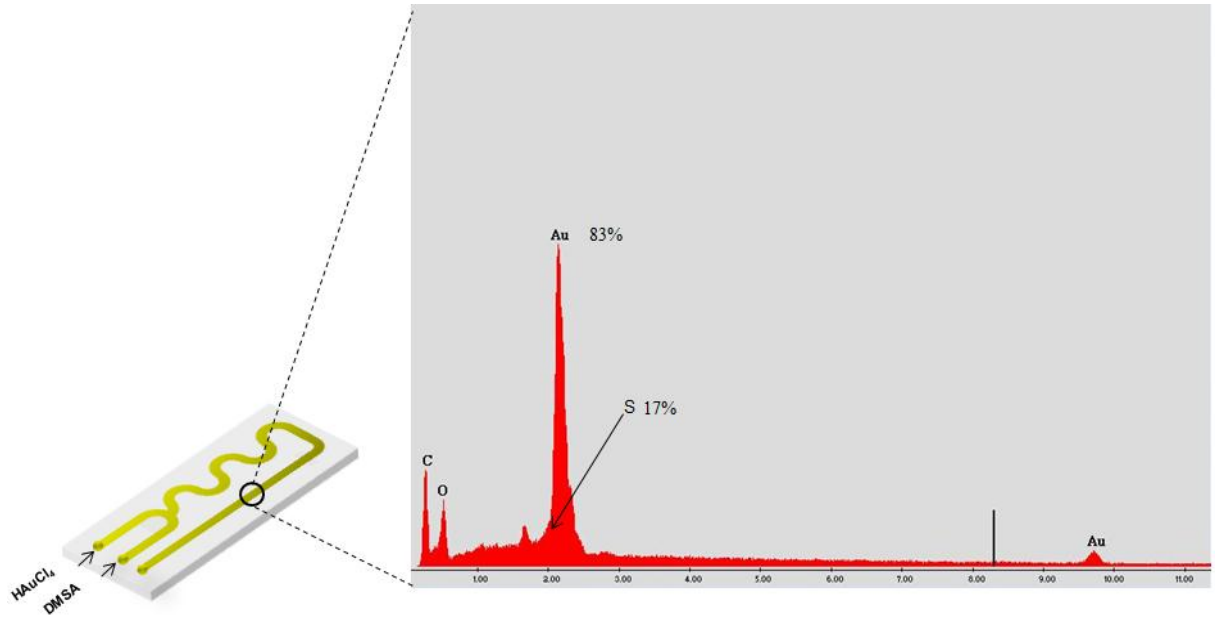

Figure 4.4: EDAX elemental analysis of gold structures from Figure 4.1

Although such hemispherical shapes for gold were previously reported, this was a first-time report on formation of such structures without using any template. The gold hemispheres were ~ 3 μm in size and have a rough porous surface. The hemispherical structures seem to be formed from the fusion of numerous smaller-sized particles that generate occasional pores on its curved surface. The irregular rough surface was usually preferred for their high-surface area and was commonly found in electrodes used for catalysis.

Since the morphology of the gold formed could be affected by several factors such as the time of $Au_xS_y^-$ deposition and the flow rates within the channels, the time intervals of deposition were varied keeping the flow-rate constant (*i.e.* 1 ml/h) and the morphology of the resultant structures were explored.

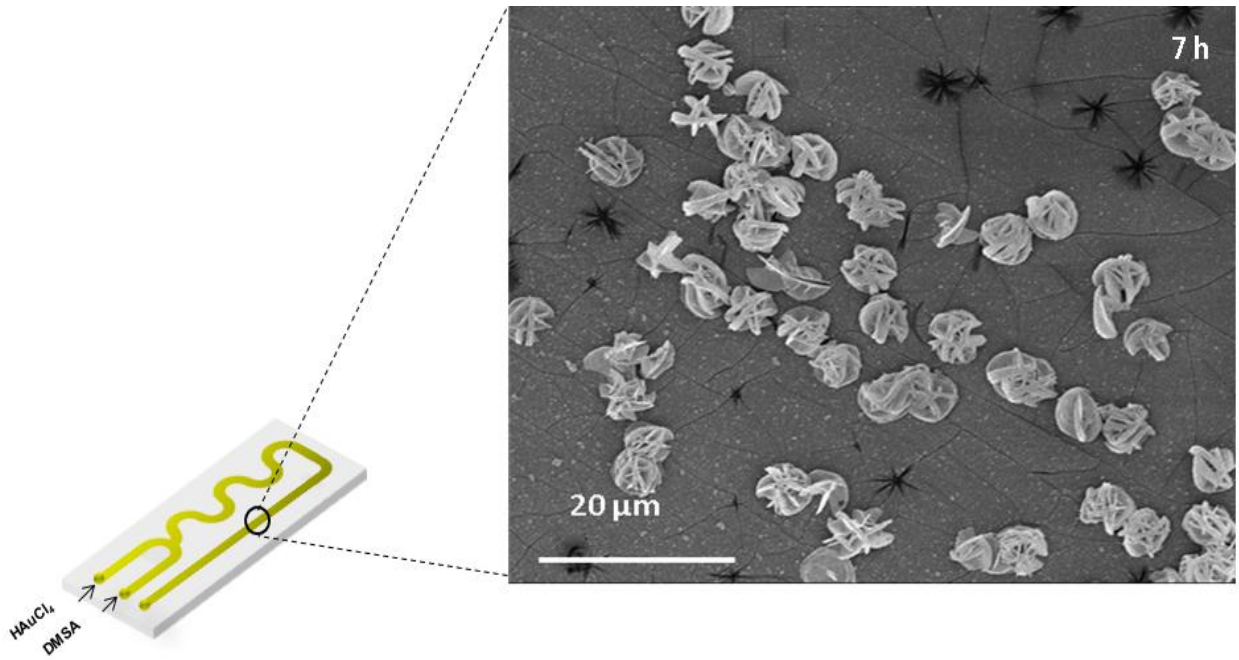

Figure 4.5: Gold structures formed at 1 ml/h flow rate for 7 h flow time

Figure 4.5 shows the SEM image for 7 h deposited sample that shows the structures with incompletely formed hemispheres. However, the size of the structures resembles those of the finally formed hemispheres deposited at 9 h duration.

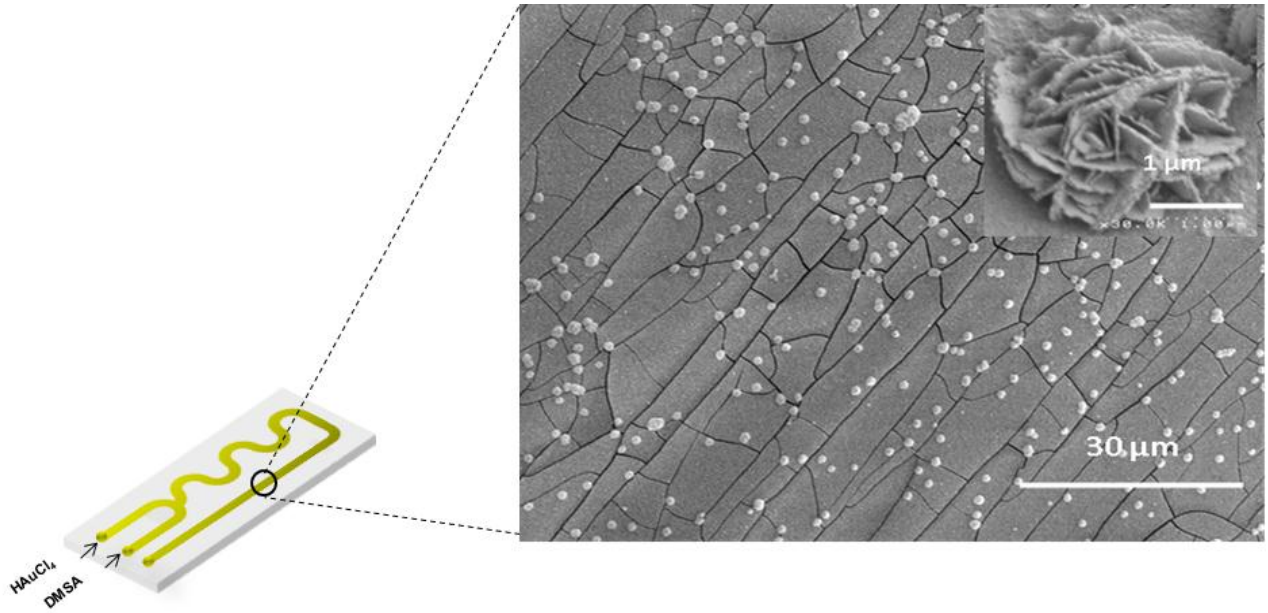

Figure 4.6: Gold structures formed at 1 ml/h flow rate for 5 h flow time

Figure 4.6 shows a flower-like morphology of gold structures which was formed at 5 hour deposition time. The structures were ~ 3 μm and have corrugated petal-like features resembling flower morphology. Inset of Figure 4.6 shows the closer view of the same micro-flowers with multiple grooves of size 100 – 200 nm rendering them porous.

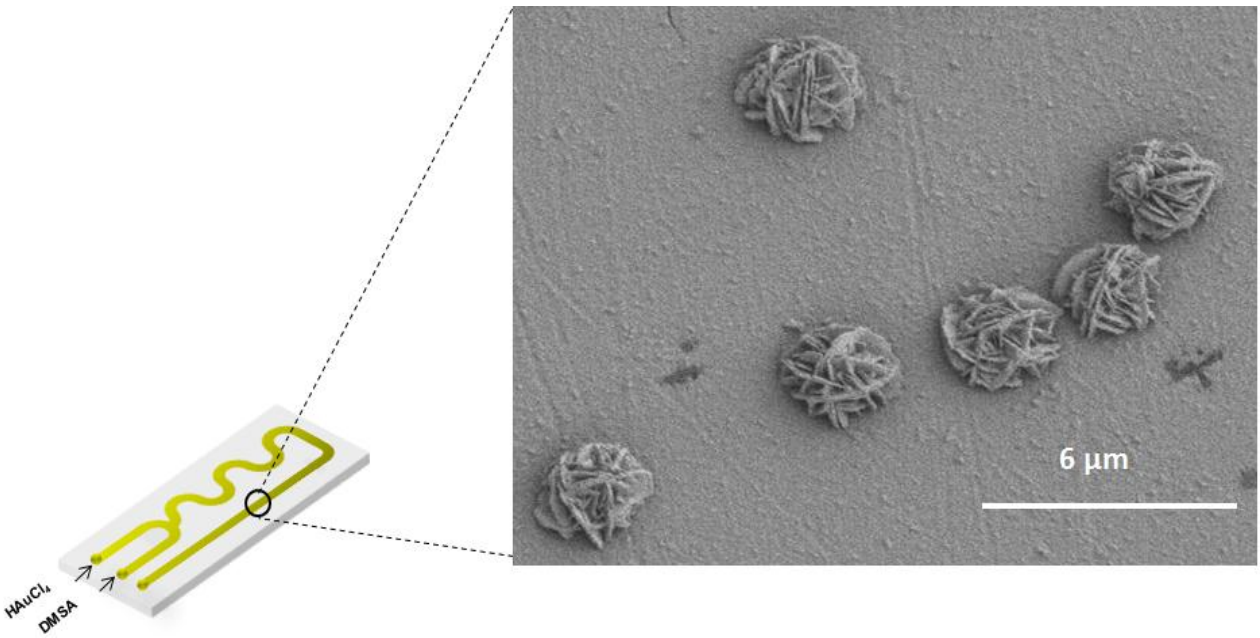

Figure 4.7: Magnified image of the gold structures formed at 1 ml/h flow rate for 5 h flow time

Figure 4.7 shows similar micro-flowers with corrugated petals that formed at 5 h duration. However, the structures shown in Figure 4.7 were formed from their preliminary stage of formation at 3 h deposition time as shown in Figure 4.8; which was subsequently formed from the random-shaped nanoparticles of 300 nm size observed at 1 h deposition time shown in Figure 4.9. The SEM images taken after depositing the gold at 1 ml/h for 1 hour shows a thin layer of gold film formed in the millifluidic reactor before the nucleation of the gold structures was initiated, (Figure 4.9).

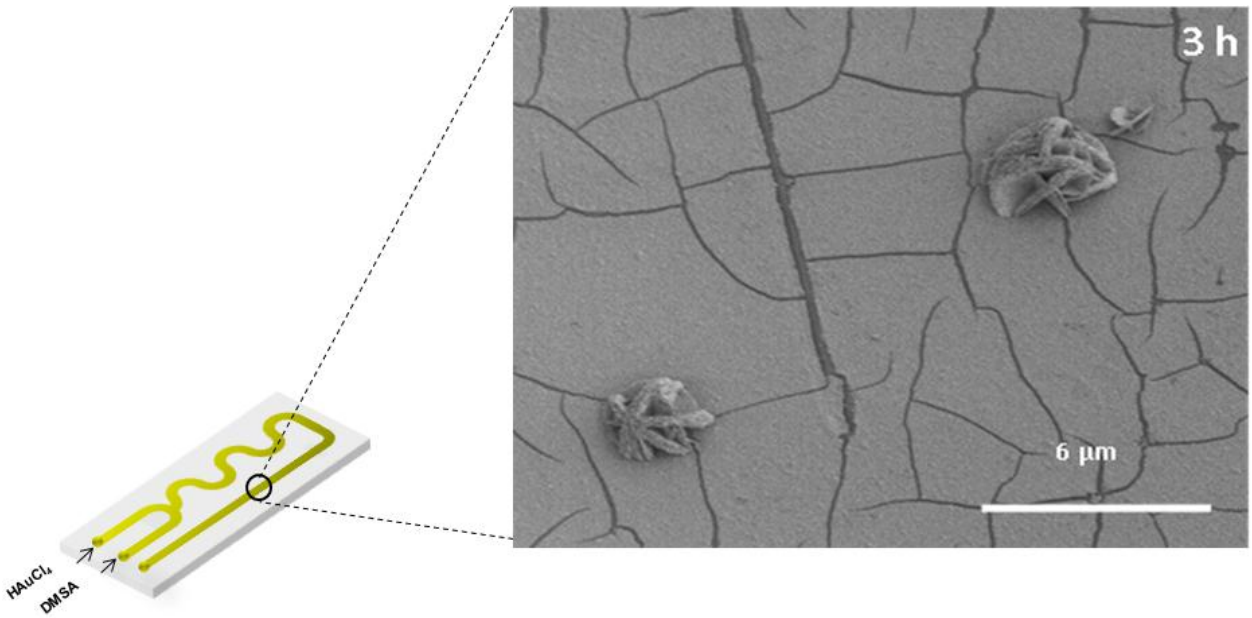

Figure 4.8 Gold structures formed at 1 ml/h flow rate for 3 h flow time

A complete understanding of these formed structures with respective deposition times indicate that the micro-hemispherical morphology of gold was gradually evolved from smaller-sized nanoparticles through the intermediate flower-like morphology.

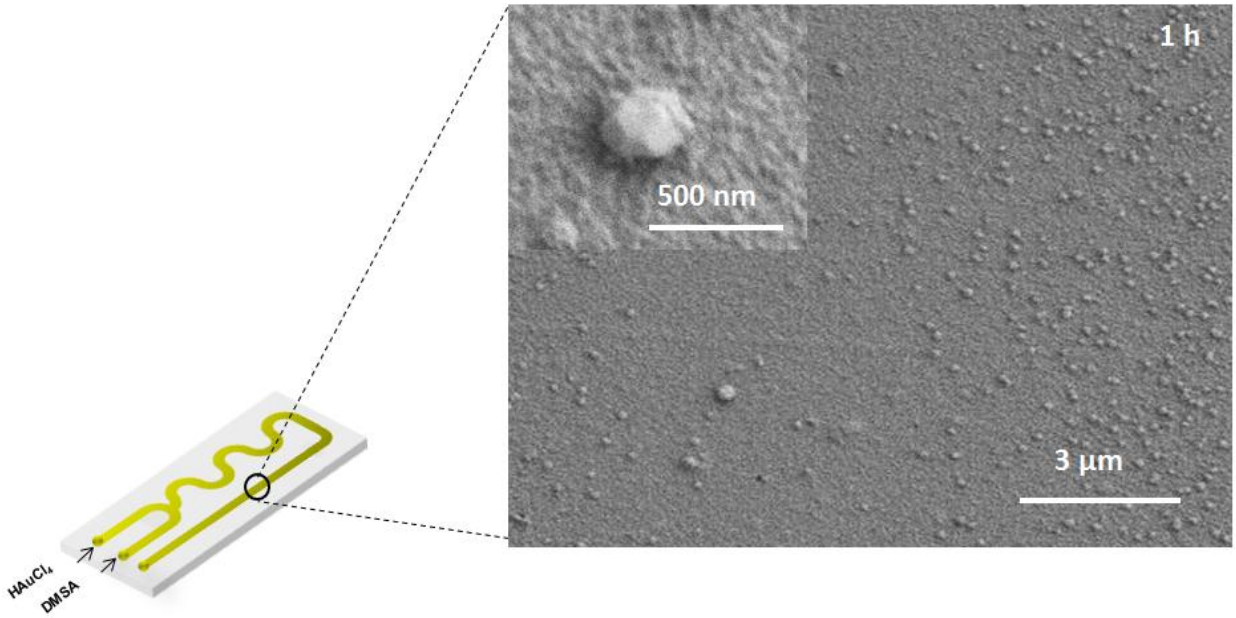

Figure 4.9 Gold structures formed at 1 ml/h flow rate for 1 h flow time

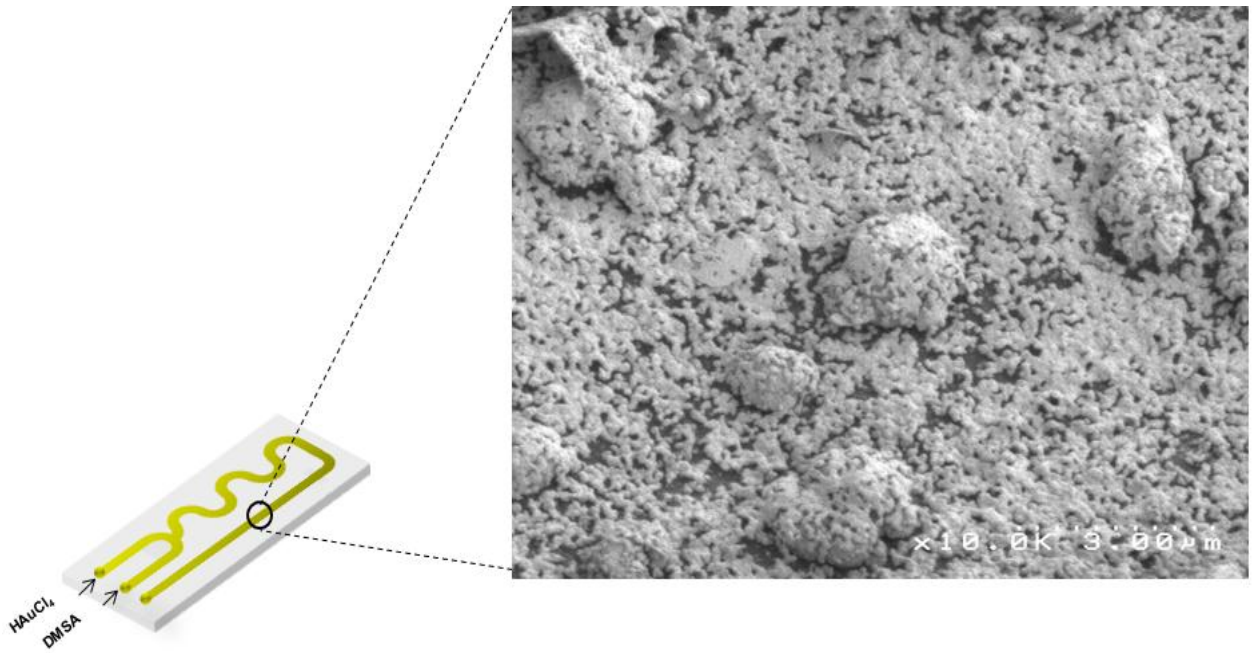

Figure 4.10: Gold structures formed at 1 ml/h for 9 hour

The formation of the gold structures was also carried out in a millifluidic chip made with a different polymer, ULTEM (polyetherimide) to understand the effect of polymer on the morphology of the gold structures.. These structures formed within the ULTEM millifluidic chip were observed under SEM. However, the structures were different than that of the PET millifluidic chip. Hemispherical structures overlaid by smaller spheres were observed in the case of ULTEM polymer (Figure 4.10).

4.1.2 X-ray absorption near edge spectroscopy (XANES)

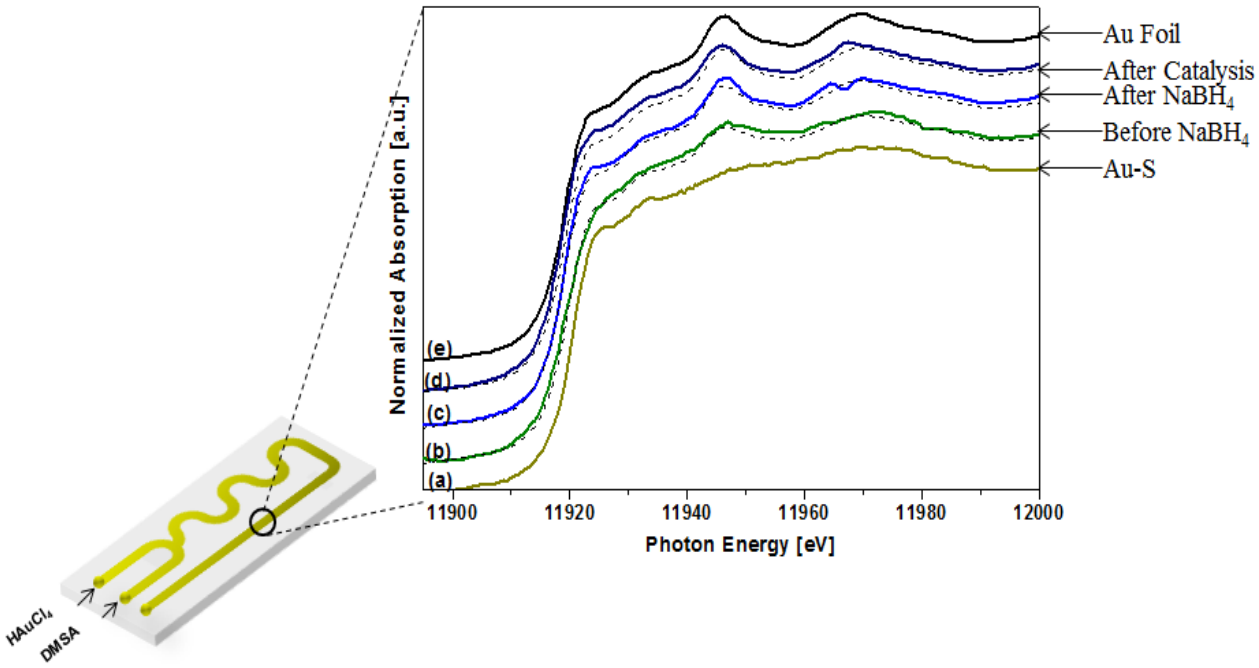

Fig 4.11: Au L3-edge X-ray absorption near edge spectroscopy (XANES) data

To understand the chemical nature of the deposited structures at different stages within the channels, three different samples *viz.* before $NaBH_4$ reduction, after $NaBH_4$ reduction and after the catalysis reactions were chosen for analysis using X-ray absorption spectroscopy (XAS). Figure 4.11 shows the Au L3-edge X-ray absorption near edge spectroscopy (XANES) data of the three samples together and the references for bulk gold and gold sulfide with their fits using linear combination fitting. The linear combination fitting approach yields 50% Au-S and 50% Au-Au bonding for the sample before borohydride reduction. These values were expected since the gold precursor, $HAuCl_4$ was initially reacting with DMSA resulting in the formation of gold sulfide, $Au_xS_y^-$ with both Au-S and Au-Au linkages. The sample after borohydride reduction has only 17% Au-S and 83% Au-Au bonding (Figure 4.4), which suggests the reduction effect of borohydride on Au-S. Finally, there was only Au-Au bonding and no Au-S bonding and very

similar to bulk gold for the sample after the catalysis reaction. This complete conversion of Au-S to Au-Au was aided by the extra borohydride added while performing catalysis reactions.

4.1.3 3-D X-ray tomography

The width and thickness of the deposited film was controlled by varying the flowing time of reagents keeping the flow-rate constant within the channels. Figure 4.12 shows the 3-D X-ray tomography images of the gold structures formed at 1 h, 5 h and 9 h flow time respectively.

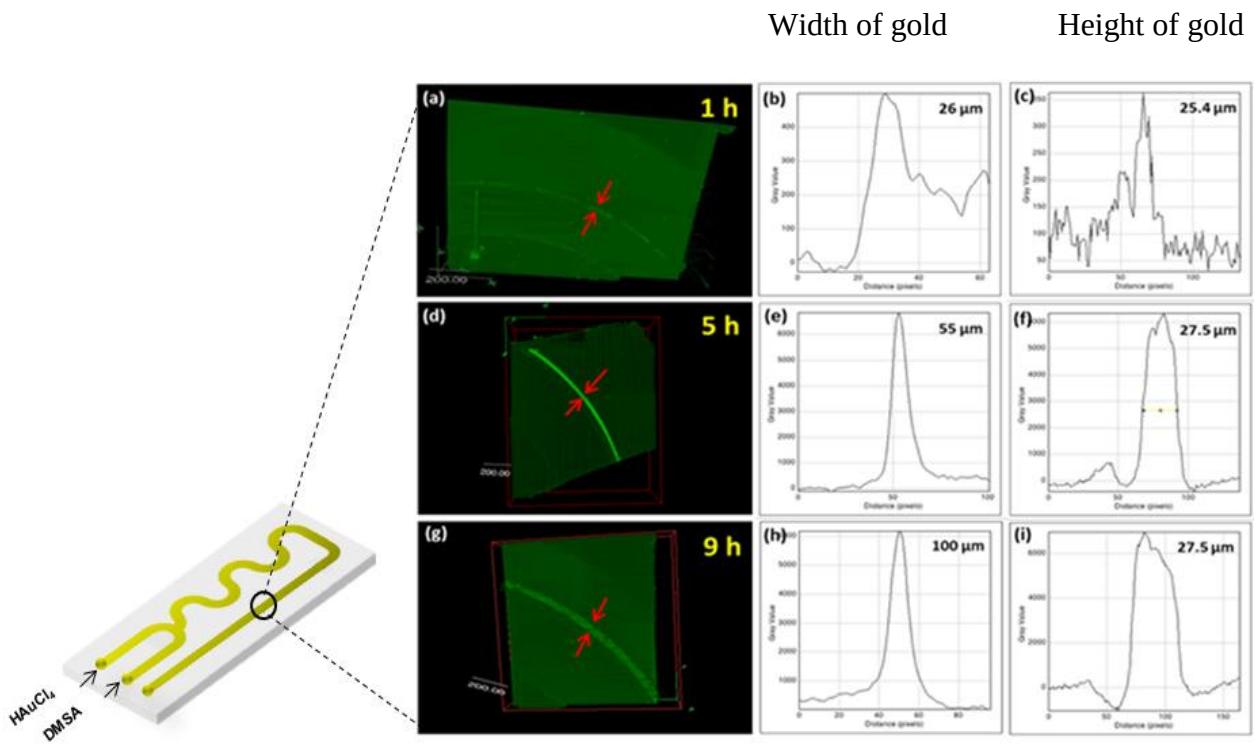

Fig 4.12: 3-D X-ray tomography width and height profiles of gold formed at 1 h (A, B and C), 5 h (D, E and F) and 9 h (G, H and I) flow time

The measured width and depth profiles (Figure 4.12) increase gradually with the time of deposition. The film width gradually increases from 26 µm for gold embedded for 1 h flow time

(Figure 4.12B) to 100 µm for gold embedded for 9 h flow time (Figure 4.12H). However, the thickness gets saturated at 27.5 µm for gold embedded for 5 h flow time of deposition (Figure 4.12F) The gold structures embedded at different flow time were probed using the scanning electron microscope (SEM) for analyzing their topographic details. Since the morphology of the deposited gold structures could be affected by several factors (such as the flow-rates and deposition time), the flow-rate in all the experiments was kept constant (*i.e.* 1 ml/h) and the deposition time was varied to explore their morphology.

4.2 Reproducibility of the gold structures within the millifluidic reactor

To investigate the reproducibility of the gold structures within the millifluidic channel, two different millifluidic chips, which had standard deposition of gold structures resulting from 1 ml/h flow rate for 9 h flow time was analyzed using SEM. The SEM images (Figure 4.13 and 4.14) revealed that the gold within the two millifluidic reactors had the same morphology which proved the coating of gold within the millifluidic channels to be reproducible.

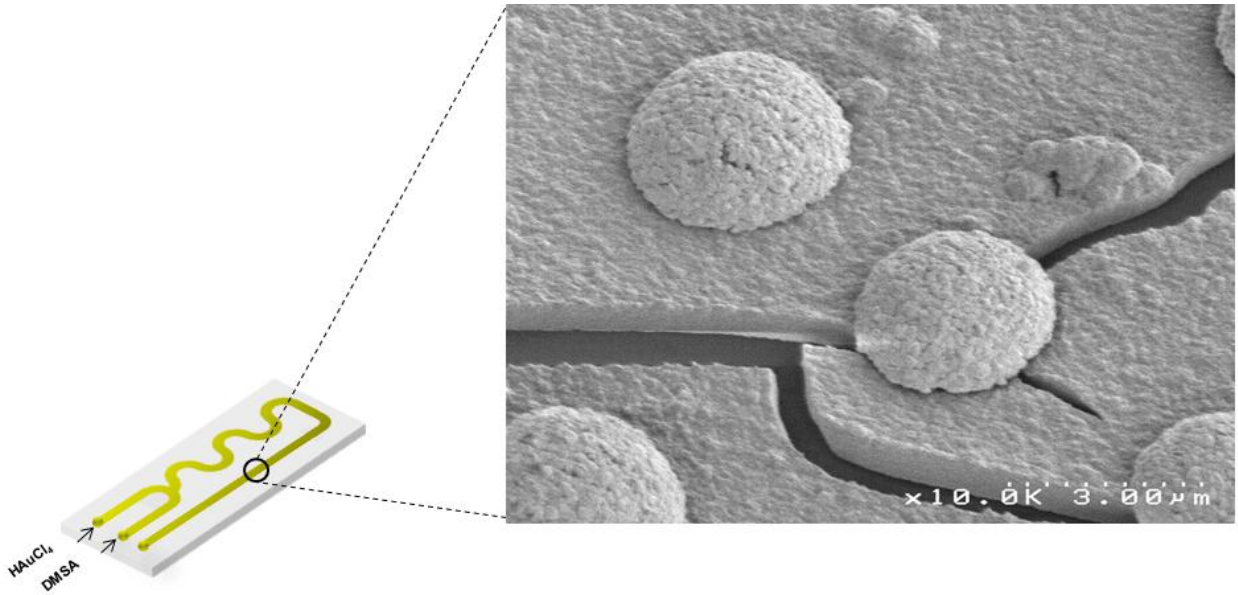

Figure 4.13: Gold structures formed at 1 ml/h flow rate for 9 h flow time

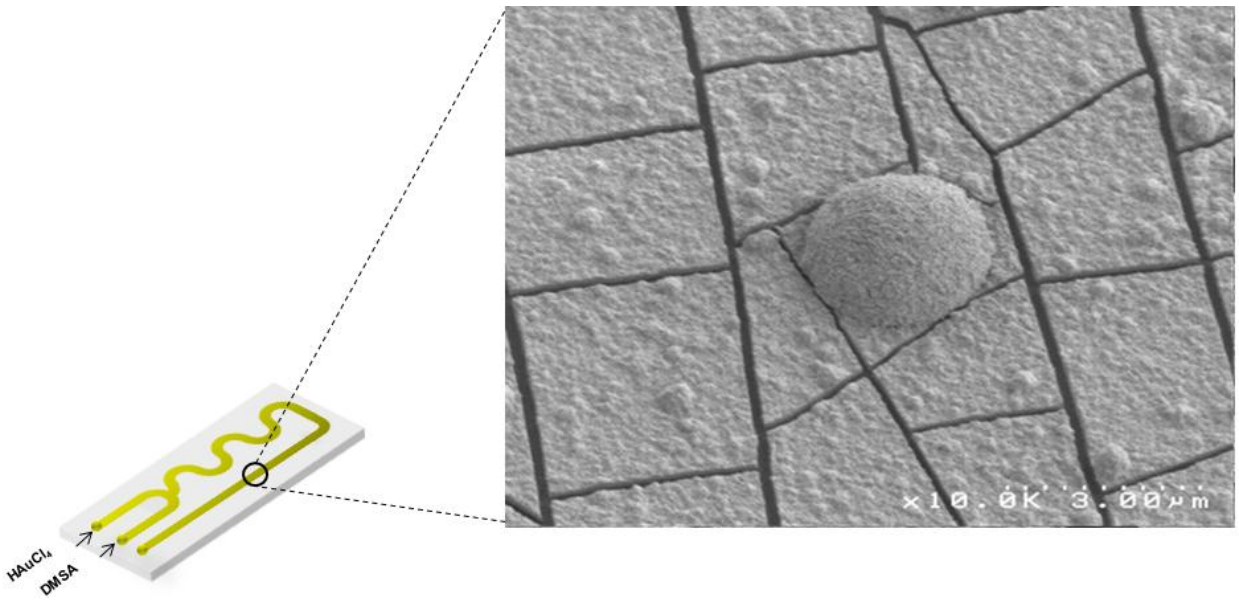

Figure 4.14: Gold structures formed at 1 ml/h flow rate for 9 h flow time

4.3 Synthesis of silver structures within millifluidic reactor

To demonstrate the generic nature of morphology control of structures with metals other than gold, similar experiment were performed using silver. However, silver formed macroporous structures (Figure), which were not similar to the gold structures formed under same conditions.

4.3.1 Experimental procedure

4:1 molar ratio of Lipoic acid:$NaBH_4$ solution was prepared by dissolving 26.3 mg of lipoic acid powder and 1.2 mg of pure sodium borohydride and mixed well in 10 ml of nanopure water until a clear solution was observed. In this step, the lipoic acid in water was reduced to form soluble dihydrolipoic acid (DHLA). 25 mM of $AgNO_3$ solution was prepared by dissolving 0.424 g of $AgNO_3$ in 100 ml nanopure water. Standard solution (10 mM) of $NaBH_4$ was prepared by dissolving 11.34 mg of $NaBH_4$ in 30 ml of Nanopure water. 10 ml of the $AgNO_3$ and DHLA

solutions were taken into two separate syringes each and were connected to the chip's manifold. The experiment was carried out by flowing of $AgNo_3$ and DHLA solutions at 1 ml/h for 9 hours. The as-formed silver within the millifluidic reactor was washed with $NaBH_4$ at 5 ml/h for 15 minutes and with nanopure water at 5 ml/h for 30 minutes respectively.

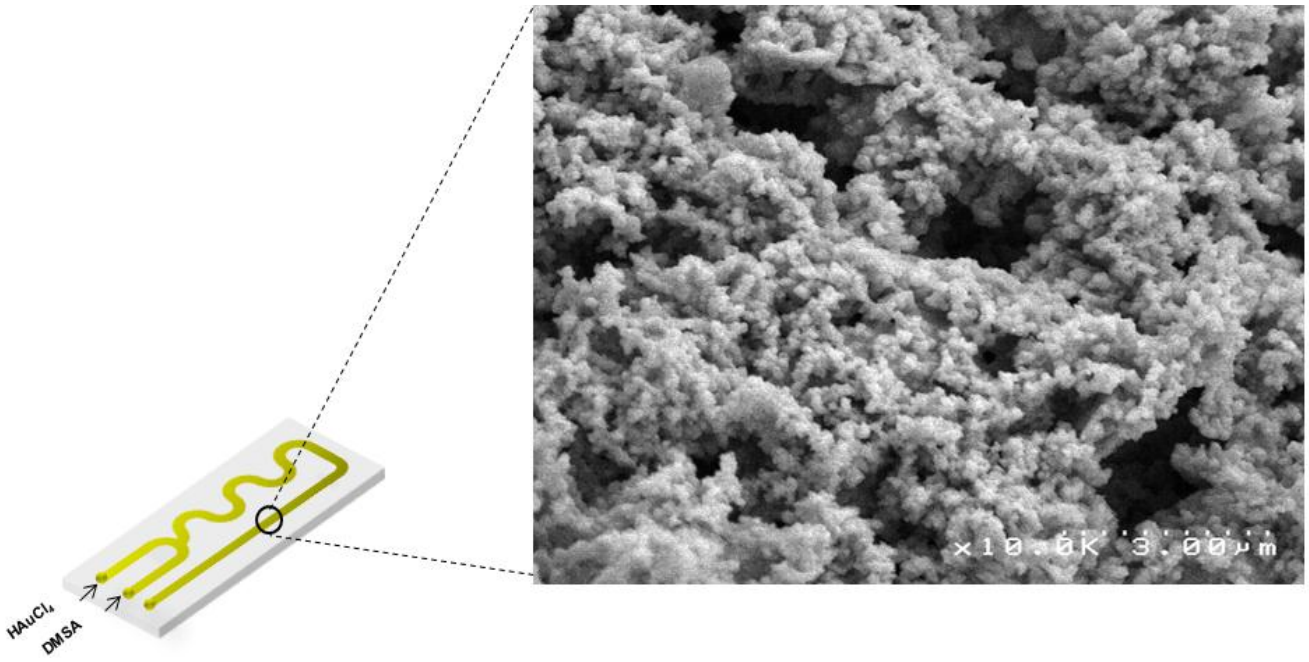

Fig 4.15: SEM image of silver microstructures formed at 1 ml/h for 9 hours

5. CATALYTIC ACTIVITY OF THE GOLD STRUCTURES FOR KINETIC STUDIES

5.1 Results and discussions

The catalytic activity of the gold coated within the millifluidic reactor was tested initially before the kinetic experiments were done. It was observed that the catalytic behavior of the gold structures within the millifluidic channel was active after treating it with 400 ml of phenolate ion solution at 5 ml/h for 4-nitrophenol reduction reaction.

5.1.1 Catalysis reactions

To prove that the gold structures deposited within the millifluidic reactor were catalytically active, two different catalytic reactions were chosen to be performed. Three different chips deposited for different times, 9 h (micro-hemispheres), 5 h (micro-flowers) and 1 h (polygonal nanoparticles) respectively at 1 ml/h were used for the purpose due to their distinctive structural differences.

5.1.1.1 Reduction of 4-nitrophenol to 4-aminophenol

The first catalysis reaction was reduction of 4-nitrophenol to 4-aminophenol. Initially 4-nitrophenol was converted to its more reactive phenolate ion species by mixing it with $NaBH_4$. The as-formed phenolate ion was later introduced into the chip to convert it into 4-aminophenol (4-AP). Figure 5.1 shows the UV-Vis spectra of the collected sample after flowing it through the Au-deposited chip. The 4-NP absorption spectrum shows a λ_{max} at 316 nm. The λ_{max} value shifts to 399 nm after mixing it with $NaBH_4$ to form phenolate ion. The phenolate ion converts to 4-aminophenol in the presence of Au catalyst and has a λ_{max} of 301 nm. In the absence of any Au

catalyst, there was negligible conversion observed for the 4-NP. However, in the presence of catalyst, it was observed that the initial peak for phenolate ion had completely diminished and a new peak corresponding to 4-aminophenol had emerged (Kuroda, 2009)

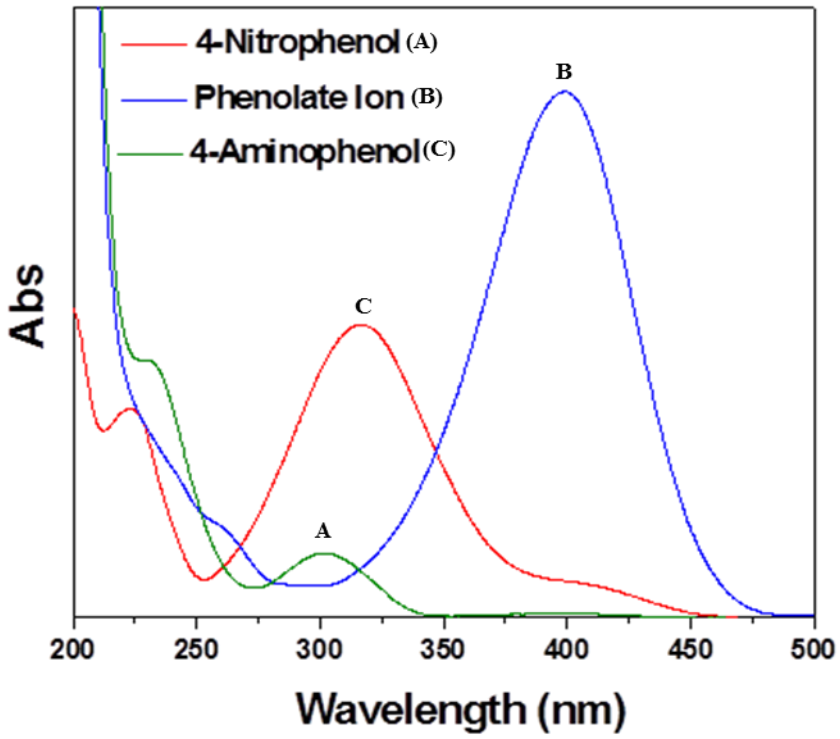

Figure 5.1: UV-Vis spectrum for standard 4-nitrophenol, 4-aminophenol and phenolate ion

To understand the optimal flow-rate for better conversion, the reaction was carried out at different flow-rates *viz.* 5, 20, 40 and 60 ml/h for both micro-hemispheres (Figure 5.2) and micro-flowers (Figure 5.3) and the corresponding reaction rates were calculated. Table 5.1 and Table 5.2 summarizes the reaction rates observed at different flow-rates for micro-hemispherical and micro-flowered gold structures respectively.

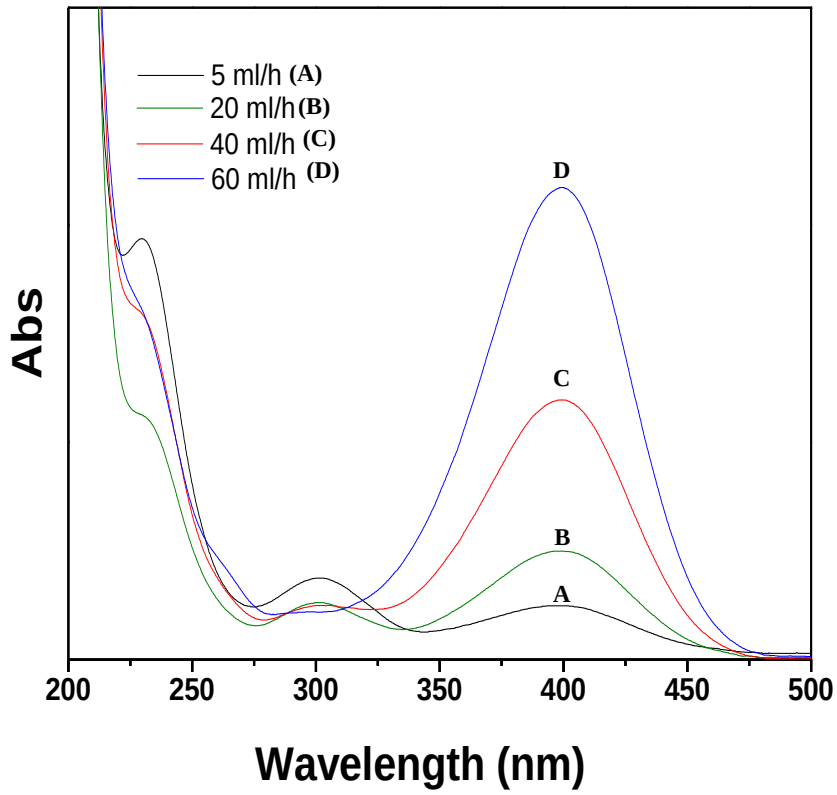

Figure 5.2: UV-Vis spectrum for 4-nitrophenol conversion reaction with micro-hemispherical gold structures formed at 1 ml/h for 9 h flow time

Table 5.1: Observed reactant depletion rates for 4-nitrophenol conversion reaction with micro-hemispherical gold structures formed at 1 ml/h for 9 h flow time

Reaction: 4-nitrophenol conversion to 4-aminophenol		
Flow-rate of reactant (ml/h)	**Observed reactant depletion rate (MS^{-1})**	
	Millifluidic channel with gold	**Millifluidic channel without gold**
5	1.13×10^{-10}	2.44×10^{-11}
20	4.03×10^{-10}	7.77×10^{-11}
40	5.38×10^{-10}	7.77×10^{-11}
60	2.40×10^{-10}	6.64×10^{-11}

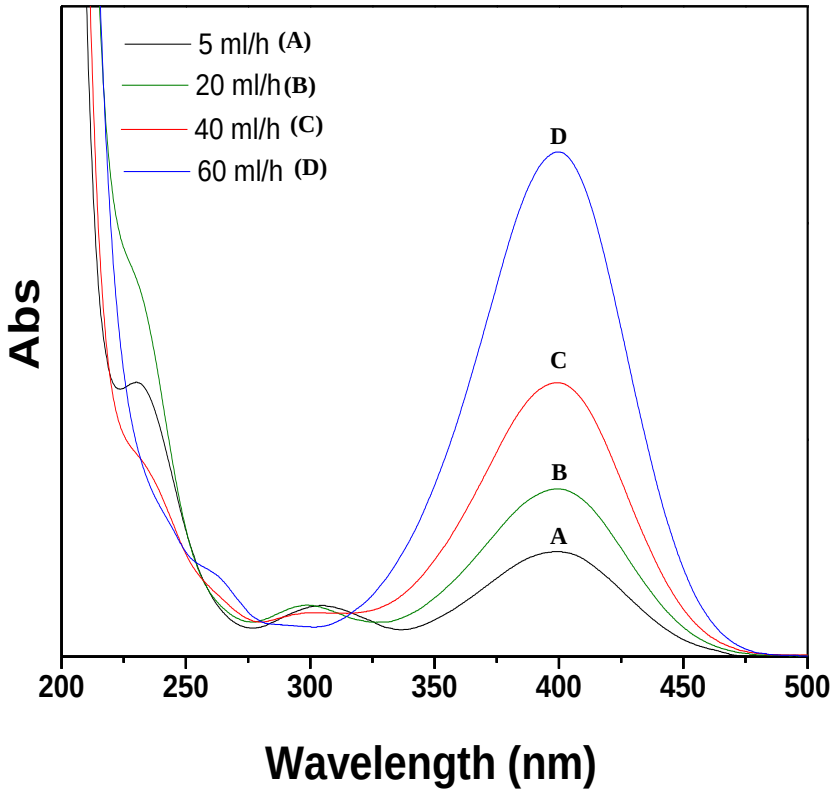

Figure 5.3: UV-Vis spectrum for 4-nitrophenol conversion reaction with micro-flowered gold structures formed at 1 ml/h for 5 h flow time

Table 5.2: Observed reactant depletion rates for 4-nitrophenol conversion reaction with micro-flower gold structures formed at 1 ml/h for 5 h flow time

Reaction: 4-nitrophenol conversion to 4-aminophenol		
Flow-rate of reactant (ml/h)	**Observed reactant depletion rate (MS^{-1})**	
	Millifluidic channel with gold	**Millifluidic channel without gold**
5	1.01×10^{-10}	2.44×10^{-11}
20	3.50×10^{-10}	7.77×10^{-11}
40	5.11×10^{-10}	7.77×10^{-11}
60	1.51×10^{-10}	6.64×10^{-11}

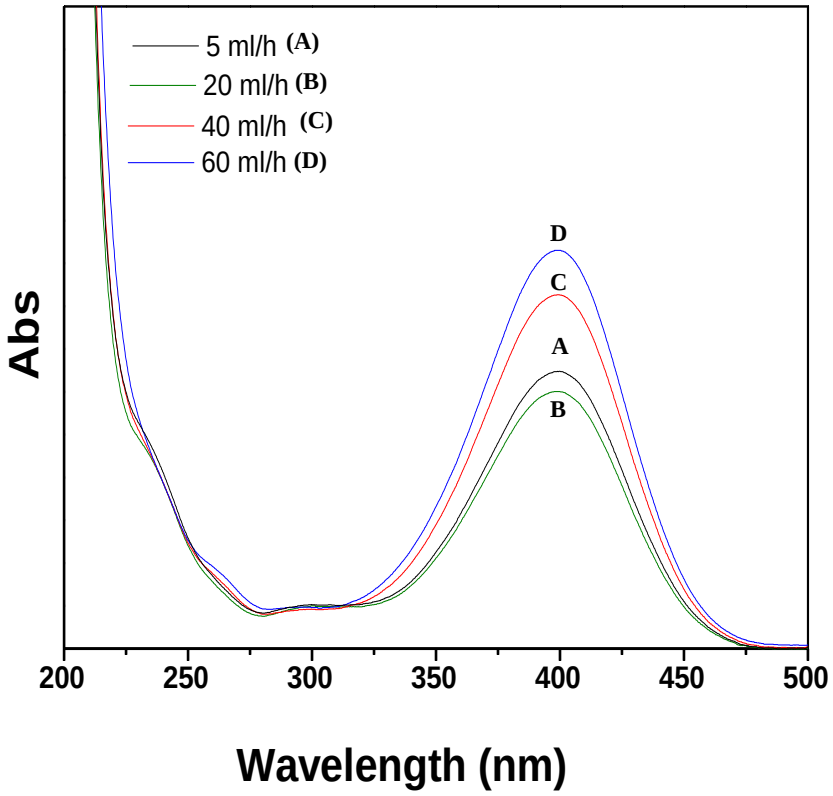

Figure 5.4: UV-Vis spectrum for 4-nitrophenol conversion reaction with gold film formed at 1 ml/h for 1 h flow time

Table 5.3: Observed reactant depletion rates for 4-nitrophenol conversion reaction with gold film formed at 1 ml/h for 1 h flow time

Reaction: 4-nitrophenol conversion to 4-aminophenol		
Flow-rate of reactant (ml/h)	**Observed reactant depletion rate (MS^{-1})**	
	Millifluidic channel with gold	**Millifluidic channel without gold**
5	6.21×10^{-11}	2.44×10^{-11}
20	2.67×10^{-10}	7.77×10^{-11}
40	3.60×10^{-10}	7.77×10^{-11}
60	4.21×10^{-10}	6.64×10^{-11}

The rate of the reaction for the reduction of 4-nitrophenol to 4-aminophenol were calculated from the calibration curves obtained using UV-Vis absorption spectra of the reactants and products for 9 hours (Figure 5.2) and 5 hours (Figure 5.3) samples respectively. The reactants were passed at different flow rates *viz.* 5, 20, 40, 60 ml/h over the gold structures, deposited at 1 ml/h for 9 and 5 hours within the millifluidic reactor. It was observed that the rate of the reaction decreased with increased flow rate. The decrease in the rate of the reaction was due to the retention time of the reactants with the gold structures within the millifluidic reactor. However the conversion was high in the case of gold structures deposited for 9 h (Table 5.1) than the 5 h (Table 5.2), which was due to the higher amount of gold available for catalysis for 9 h sample than 5 h sample. The catalysis reaction was also carried out with the gold structures formed at 1 h time and the corresponding reaction rates were calculated. From the calibration curves and calculations it was observed that the rate of the reaction follows the trend: 9 h > 5 h > 1 h.

5.1.1.2 Reduction of Potassium hexacyanoferrate (III) to Potassium hexacyanoferrate (II)

The second catalysis reaction was Potassium hexacyanoferrate (III) to Potassium hexacyanoferrate (II) conversion. Potassium hexacyanoferrate (III) solution was initially mixed with $NaBH_4$ and the resultant solution was passed through the gold-deposited chip. Figure 5.5 shows the UV-Vis spectra of the reactant Potassium hexacyanoferrate (III) and the collected product Potassium hexacyanoferrate (II). Potassium hexacyanoferrate (III) has a λ_{max} of 419 nm, which was totally converted to Potassium hexacyanoferrate (II) that has a λ_{max} of 321 nm (Carregal, 2009).

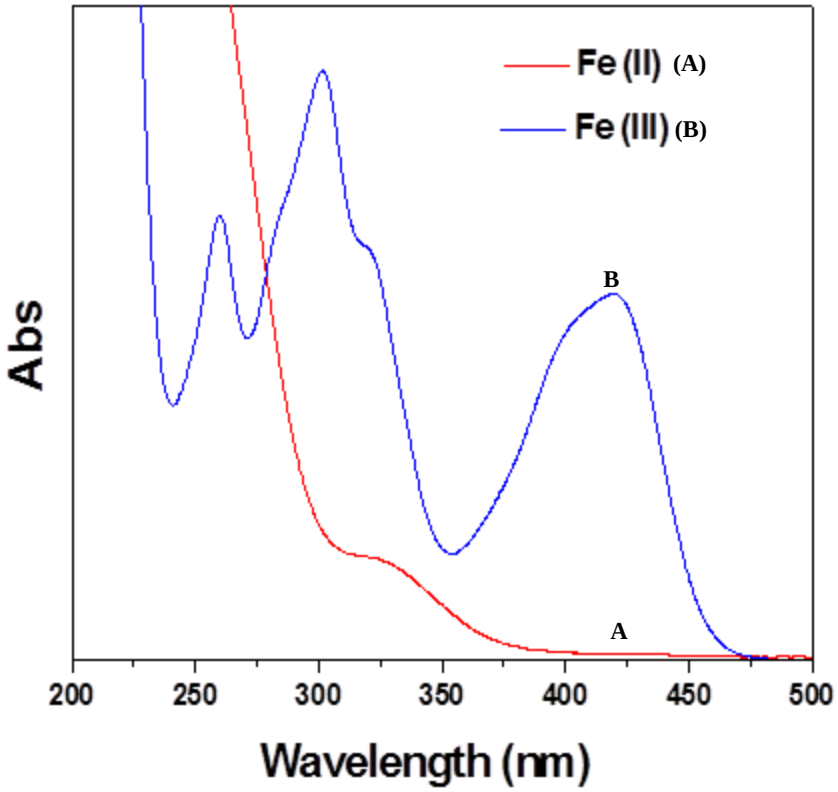

Figure 5.5: UV-Vis spectrum for standard Potassium hexacyanoferrate (III) and Potassium hexacyanoferrate (II)

To understand the optimal flow-rate for better conversion, the reaction was carried out at different flow-rates *viz.* 5, 20, 40 and 60 ml/h for both micro-hemispheres (Figure 5.6) and micro-flowers (Figure 5.7) and the corresponding reaction rates were calculated. Table 5.4 and Table 5.5 summarize the reaction rates observed at different flow-rates for micro-hemispherical and micro-flowered gold structures respectively.

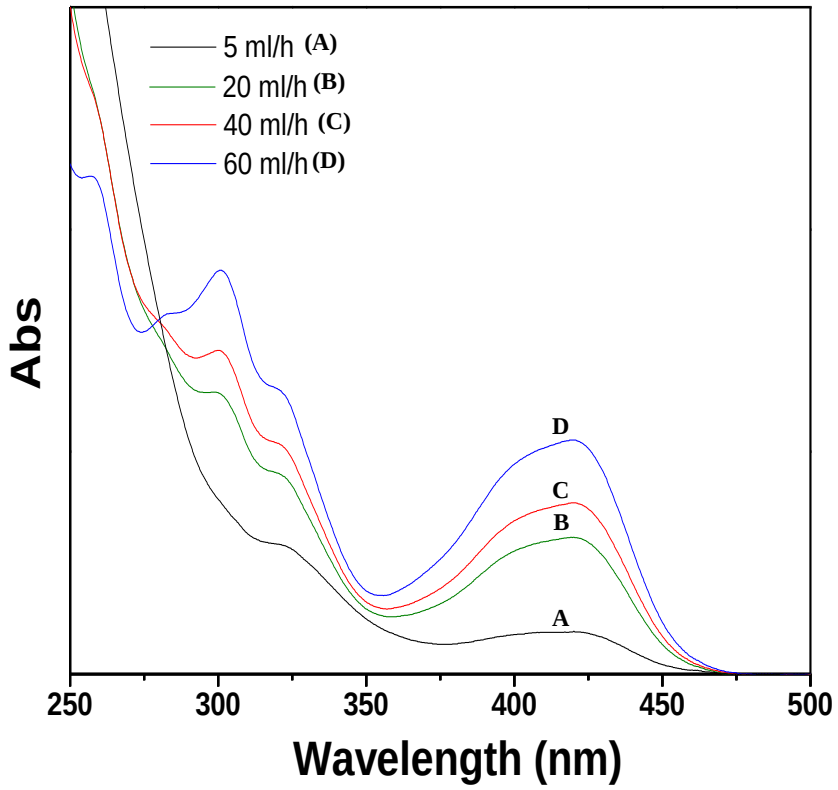

Figure 5.6: UV-Vis spectrum for Potassium hexacyanoferrate (III) conversion reaction with micro-hemispherical gold structures formed at 1 ml/h for 9 h flow time

Table 5.4: Observed reactant depletion rates for Potassium hexacyanoferrate (III) conversion reaction with micro-hemispherical gold structures formed at 1 ml/h for 9 h flow time

Reaction: Potassium hexacyanoferrate (III) conversion to Potassium hexacyanoferrate (II)		
Flow-rate of reactant (ml/h)	**Observed reactant depletion rate (MS^{-1})**	
	Millifluidic channel with gold	**Millifluidic channel without gold**
5	9.82×10^{-10}	1.40×10^{-10}
20	2.40×10^{-9}	3.33×10^{-10}
40	3.82×10^{-9}	3.99×10^{-10}
60	2.73×10^{-9}	2.15×10^{-10}

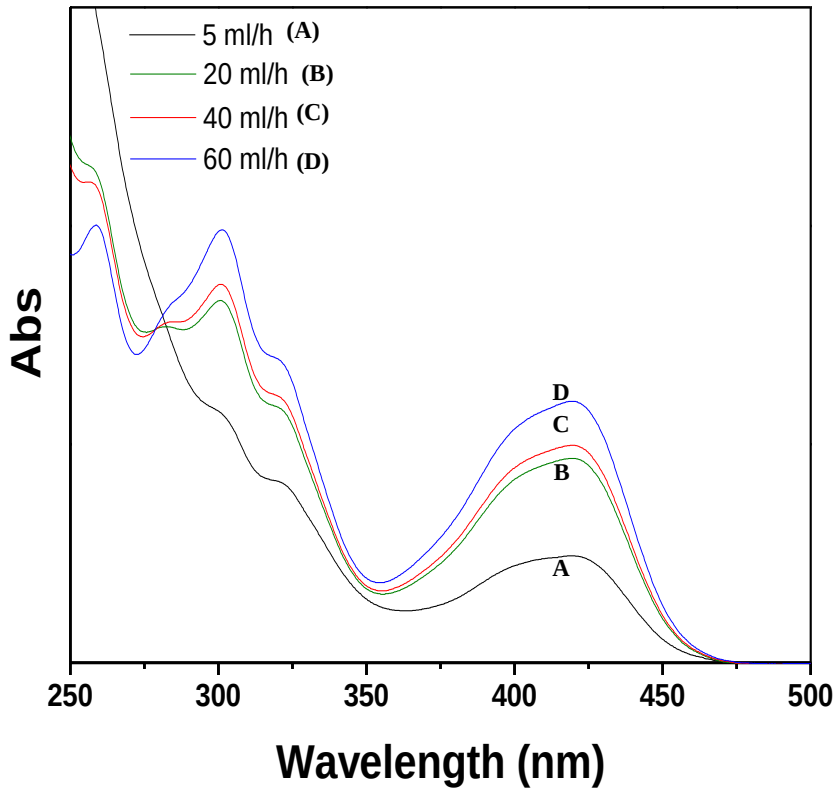

Figure 5.7: UV-Vis spectrum for Potassium hexacyanoferrate (III) conversion reaction with micro-flowered gold structures formed at 1 ml/h for 5 h flow time

Table 5.5: Observed reactant depletion rates for Potassium hexacyanoferrate (III) conversion reaction with micro-flowered gold structures formed at 1 ml/h for 5 h flow time

Reaction: Potassium hexacyanoferrate (III) conversion to Potassium hexacyanoferrate (II)		
Flow-rate of reactant (ml/h)	**Observed reactant depletion rate (MS^{-1})**	
	Millifluidic channel with gold	**Millifluidic channel without gold**
5	7.20×10^{-10}	1.40×10^{-10}
20	2.89×10^{-9}	3.33×10^{-10}
40	2.23×10^{-9}	3.99×10^{-10}
60	1.22×10^{-9}	2.15×10^{-10}

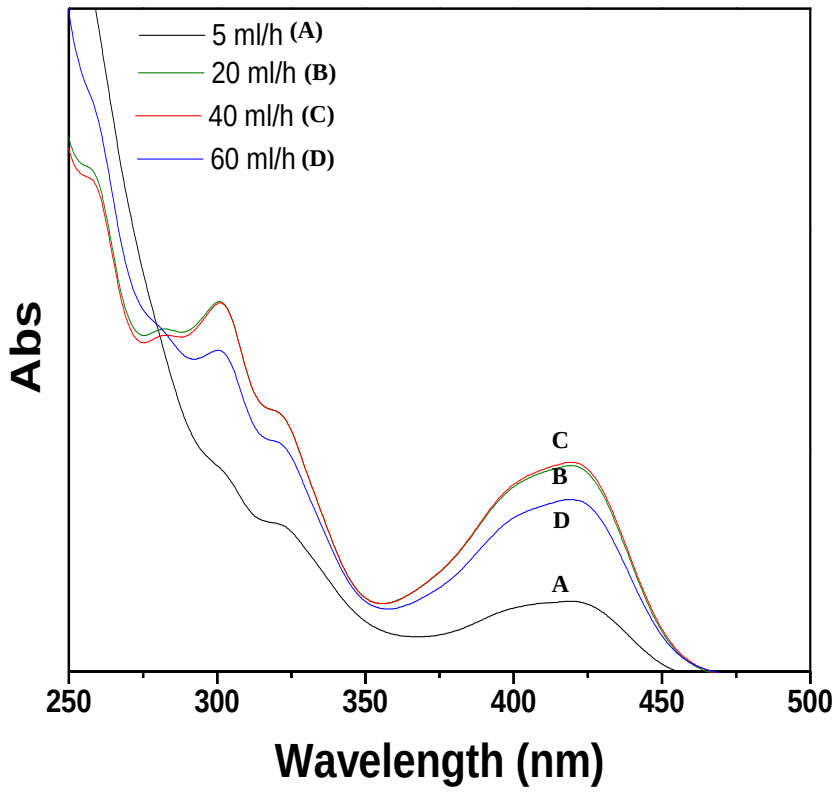

Figure 5.8: UV-Vis spectrum for Potassium hexacyanoferrate (III) conversion reaction with gold film formed at 1 ml/h for 1 h flow time

Table 5.6 Observed reactant depletion rates for Potassium hexacyanoferrate (III) conversion reaction with gold film formed at 1 ml/h for 1 h flow time

Reaction: Potassium hexacyanoferrate (III) conversion to Potassium hexacyanoferrate (II)		
Flow-rate of reactant (ml/h)	**Observed reactant depletion rate (MS^{-1})**	
	Millifluidic channel with gold	**Millifluidic channel without gold**
5	8.72×10^{-10}	1.40×10^{-10}
20	3.50×10^{-9}	3.33×10^{-10}
40	2.57×10^{-9}	3.99×10^{-10}
60	5.61×10^{-9}	2.15×10^{-10}

The rate of the reaction for the reduction of Potassium hexacyanoferrate (III) to Potassium hexacyanoferrate (II) were calculated from the calibration curves obtained using UV-Vis absorption spectra of the reactants and products for 9 hours (Figure 5.6) and 5 hours (Figure 5.7) respectively. When the reactants were passed through the gold structures deposited at 1 ml/h for 9 and 5 hours within the millifluidic reactor at different flow rates viz. 5, 20, 40, 60 ml/h, there was a decrease in the rate of the reaction when the flow rate was increased. The decrease in the rate of the reaction with respective to the flow rate was due to the retention time of the reactants with the gold structures within the millifluidic reactor. However the conversion was high in the case of gold structures deposited for 9 hours (Table 5.4) than the 5 hours (Table 5.5). This was due to more amount of gold with higher surface area and active sites in the 9 h deposited gold structures. The same reaction was carried out with the gold deposited at 1 ml/h for 1 hour within the millifluidic channels for calculating the rate of the reaction. From the UV-Vis spectrum and calculations it was observed that the rate of the reaction of follows the trend: 9 hours > 1 hour > 5 hours.

5.2 Other catalytic reactions attempted

In addition to the catalysis reactions discussed above, biomass conversion reactions were also carried out within the millifluidic reactor under different reaction conditions. Hydroxymethyl furfural, a carbon-neutral feedstock for fuels and chemicals was used to check the catalytic activity of gold structures. Conversion of HMF involved two types of reactions via oxidation and reduction. HMF was mixed with various volumes of NaOH and TBHP and treated with oxygen before passing through the millifluidic reactor at two different temperatures (22 °C and 60 °C). The products collected were analyzed using the UV-Vis spectrum for FDCA. From

the UV-Vis spectra it was understood there was no significant conversion of HMF at both temperatures. Reduction of HMF was also carried out by treating the solution with $NaBH_4$. This reaction condition was ruled out since there was total completion of the HMF reduction when higher concentration of $NaBH_4$ was added. Reduction of Formic acid, levulinic acid and succinic acid were also carried out which gave unfavorable results.

5.3 Conclusions

Reduction of 4-nitrophenol to 4-aminophenol and Potassium hexacyanoferrate (III) to Potassium hexacyanoferrate (II) reactions were carried out with the gold deposited within the millifluidic reactor at 1 ml/h for 9, 5 and 1 hour respectively. The rate of the reaction for the gold deposited for different time interval were calculated by flowing the reactant at different flow rates viz. 5, 20, 40, 60 ml/h and the products were analyzed using the UV-Vis spectrophotometer which proved the gold within the millifluidic reactor was catalytically active. However, the conversion of the reactants to products in 4-nitrophenol and Ferricyanide conversion reactions were very less without the presence of gold within the millifluidic channel.

6. CONCLUSIONS AND FUTURE RECOMMENDATIONS

6.1. Conclusions

Successful study of synthesis of gold microstructures within the millifluidic reactor was carried. The as-formed gold structures were characterized using X-ray absorption spectroscopy, 3-D X-ray tomography and Scanning electron microscopy (SEM) to understand the growth and morphology at different deposition time. Further, the gold structures were found to be catalytically active towards reduction of 4-nitrophenol to 4-aminophenol and Potassium hexacyanoferrate (III) to Potassium hexacyanoferrate (II) reactions.

6.2. Future applications

Future research will be directed towards using millifluidic systems for various biomass conversion reactions. A thorough study of these reactions at different spatial intervals will be studied using *in situ* UV-Vis, FTIR spectroscopy probes and small angle X-ray spectroscopy. Synchrotron radiation based spectroscopy tools, especially XAS, in-conjunction with millifluidic systems will be carried out for *in situ* time resolved experiments that provides an opportunity for probing the structure and dynamics of the reactions with atomic precision. Catalysts other than gold such as silver, copper, platinum, palladium etc. will also be studied for further catalytic applications. This research provides potential opportunities for continuous flow catalysis as well as for time resolved analysis of the catalytic processes in future.

REFERENCES

1. Catalyst design and preparation for industrial applications. (1996). *Applied Catalysis A: General, 139*(1–2).

2. Alerasool, S. (1997). Symposium on Catalyst Design and Preparation for Industrial Applications. *Applied Catalysis A: General, 154*(1–2).

3. An, K., Alayoglu, S., Ewers, T., & Somorjai, G. A. (2012). Colloid chemistry of nanocatalysts: A molecular view. *Journal of Colloid and Interface Science, 373*(1), 1-13.

4. Baer, D. R., & Engelhard, M. H. (2010). XPS analysis of nanostructured materials and biological surfaces. *Journal of Electron Spectroscopy and Related Phenomena, 178–179*(0), 415-432.

5. Biay, I., Dessalces, G., Hypolite, C., Kolenda, F., & Reymond, J. P. (1991). Illustration of Process Scale-Up in Heterogeneous Catalyst Preparation. In P. A. J. P. G. G. Poncelet & B. Delmon (Eds.), *Studies in Surface Science and Catalysis* (Vol. Volume 63, pp. 1-17)

6. Biswas, S., Miller, J. T., Li, Y., Nandakumar, K., & Kumar, C. S. S. R. (2012). Developing a Millifluidic Platform for the Synthesis of Ultrasmall Nanoclusters: Ultrasmall Copper Nanoclusters as a Case Study. *Small, 8*(5), 688-698.

7. Campanati, M., Fornasari, G., & Vaccari, A. (2003). Fundamentals in the preparation of heterogeneous catalysts. *Catalysis Today, 77*(4), 299-314.

8. Cansell, F., & Aymonier, C. (2009). Design of functional nanostructured materials using supercritical fluids. *The Journal of Supercritical Fluids, 47*(3), 508-516.

9. Carregal-Romero, S., Pérez-Juste, J., Hervés, P., Liz-Marzán, L. M., & Mulvaney, P. (2009). Colloidal Gold-Catalyzed Reduction of Ferrocyanate (III) by Borohydride Ions: A Model System for Redox Catalysis. *Langmuir, 26*(2), 1271-1277.

10. Chen, S.-P., Yu, X.-D., Xu, J.-J., & Chen, H.-Y. (2011). Gold nanoparticles-coated magnetic microspheres as affinity matrix for detection of hemoglobin Alc in blood by microfluidic immunoassay. *Biosensors and Bioelectronics, 26*(12), 4779-4784.

11. Cuenya, B. R. (2010). Synthesis and catalytic properties of metal nanoparticles: Size, shape, support, composition, and oxidation state effects. *Thin Solid Films, 518*(12), 3127-3150.

12. Delmon, B. (1985). New trends in catalyst preparation. *Solid State Ionics, 16*(0), 243-249.

13. Duan, G., Cai, W., Luo, Y., Li, Z., & Li, Y. (2006). Electrochemically induced flowerlike gold nanoarchitectures and their strong surface-enhanced Raman scattering effect. [Article]. *Applied Physics Letters, 89*(21), 211905.

14. Duffy, D. C., McDonald, J. C., Schueller, O. J. A., & Whitesides, G. M. (1998). Rapid Prototyping of Microfluidic Systems in Poly(dimethylsiloxane). *Analytical Chemistry, 70*(23), 4974-4984.

15. Engl, W., Tachibana, M., Panizza, P., & Backov, R. (2007). Millifluidic as a versatile reactor to tune size and aspect ratio of large polymerized objects. *International Journal of Multiphase Flow, 33*(8), 897-903.

16. Erica Farnetti, *et al*. *"Homogeneous and heterogeneous catalyst."* Inorganic and bio-inorganic chemistry – Vol. II

17. George M. Whitesides and Abraham D. Stroock. (2001). *"Flexible Methods for Microfluidics."* Physics Today: 42-48

18. Haraldsson, K. T. (2005). *"Fabrication of Polymeric Microfluidic Devices via Photocurable Liquid Monomers, Fibre and Polymer Technology."* Department of Chemical Engineering and Technology, Royal Institute of Technology (KTH).

19. Honolka, J., Sessi, V., Zhang, J., Hertenberger, S., Enders, A., & Kern, K. (2010). Substrate dependent buffer-layer assisted growth of nanoclusters. *physica status solidi (b), 247*(5), 1063-1068

20. Kitson, P. J., Rosnes, M. H., Sans, V., Dragone, V., & Cronin, L. (2012). Configurable 3D-Printed millifluidic and microfluidic 'lab on a chip' reactionware devices. *Lab on a Chip, 12*(18), 3267-3271.

21. Kuroda, K., Ishida, T., & Haruta, M. (2009). Reduction of 4-nitrophenol to 4-aminophenol over Au nanoparticles deposited on PMMA. *Journal of Molecular Catalysis A: Chemical, 298*(1–2), 7-11.

22. Lee, S.K., X. Liu, *et al*. (2012). *"Synthesis, assembly and reaction of a nanocatalyst in microfluidic systems: a general platform."* Lab on a Chip 12(20): 4080-4084.

23. Li, Y., A. Sanampudi, *et al*. (2012). *"Size Evolution of Gold Nanoparticles in a Millifluidic Reactor."* ChemPhysChem 13(1): 177-182.

24. Li, H., & Wu, N. (2008). A large-area nanoscale gold hemisphere pattern as a nanoelectrode array. *Nanotechnology, 19*(27), 275301.

25. Liang, R.-P., Meng, X.-Y., Liu, C.-M., & Qiu, J.-D. (2011). PDMS microchip coated with polydopamine/gold nanoparticles hybrid for efficient electrophoresis separation of amino acids. *Electrophoresis, 32*(23), 3331-3340.

26. Lorber, N., Sarrazin, F., Guillot, P., Panizza, P., Colin, A., Pavageau, B., Mignard, E. (2011). Some recent advances in the design and the use of miniaturized droplet-based continuous process: Applications in chemistry and high-pressure microflows. *Lab on a Chip, 11*(5), 779-787.

27. Lorentzou, S., Zygogianni, A., Tousimi, K., Agrafiotis, C., & Konstandopoulos, A. G. (2009). Advanced synthesis of nanostructured materials for environmental applications. *Journal of Alloys and Compounds, 483*(1–2), 302-305.

28. Luo, C., Fu, Q., Li, H., Xu, L., Sun, M., Ouyang, Q., Ji, H. (2005). PDMS microfludic device for optical detection of protein immunoassay using gold nanoparticles. *Lab on a Chip, 5*(7), 726-729.

29. Marre, S., & Jensen, K. F. (2010). Synthesis of micro and nanostructures in microfluidic systems. *Chemical Society Reviews, 39*(3), 1183-1202.

30. Mayer, R. W., Quandt, T., Schimmer, K., Rotgerink, H. L., & Tacke, T. (2006). Development of tools and methods for the high-throughput preparation of commercial heterogeneous catalysts. *Studies in Surface Science and Catalysis,* Vol. Volume 162, pp. 235-242.

31. Mohamed, R. M., McKinney, D. L., & Sigmund, W. M. (2012). Enhanced nanocatalysts. *Materials Science and Engineering: R: Reports, 73*(1), 1-13.

32. Negishi, Y., & Tsukuda, T. (2003). One-Pot Preparation of Subnanometer-Sized Gold Clusters via Reduction and Stabilization by meso-2,3-Dimercaptosuccinic Acid. *Journal of the American Chemical Society, 125*(14), 4046-4047.

33. Niemantsverdriet, J. W., Engelen, A. F. P., de Jong, A. M., Wieldraaijer, W., & Kramer, G. J. (1999). Realistic surface science models of industrial catalysts. *Applied Surface Science, 144–145*(0), 366-374.

34. Oyanagi, H., Sun, Z. H., Jiang, Y., Uehara, M., Nakamura, H., Yamashita, K., Maeda, H. (2011). *In situ* XAFS experiments using a microfluidic cell: application to initial growth of CdSe nanocrystals. *Journal of Synchrotron Radiation, 18*(2), 272-279.

35. Perez .A, P. Mblinon, V. Paillard, V. Dupuis, P. Jensen, A. Hoareau, J.P. Perez, J. Tuaillon, 1995. *Nanocrystalline structures prepared by neutral Cluster beam deposition. Nanostructured materials*. Vol. 6. Pp. 43-52.

36. Podlaha E.J., Y. Li, J. Zhang, Q. Huang, A. Panda, A. Lozano-Morales, D. Davis, and Z. Guo, 2006. *Electrochemical Deposition of Nanostructured Metals*.

37. Prevenslik, T. V. (2008). Nanocatalysts by Quantum Electrodynamics Induced Electromagnetic Radiation. *Chinese Journal of Catalysis, 29*(11), 1073-1078.

38. Ravel, B., & Newville, M. (2005). Athena, Artemis, Hephaestus: data analysis for X-ray absorption spectroscopy using IFEFFIT. *Journal of Synchrotron Radiation, 12*(4), 537-541.

39. Rolland, J. P., Van Dam, R. M., Schorzman, D. A., Quake, S. R., & DeSimone, J. M. (2004). Solvent-Resistant Photocurable "Liquid Teflon" for Microfluidic Device Fabrication. *Journal of the American Chemical Society, 126*(8), 2322-2323

40. Schmidt, F. (2001). New catalyst preparation technologies—observed from an industrial viewpoint. *Applied Catalysis A: General, 221*(1–2), 15-21.

41. Shiju, N. R., & Guliants, V. V. (2009). Recent developments in catalysis using nanostructured materials. *Applied Catalysis A: General, 356*(1), 1-17.

42. Song, Y., Hormes, J., & Kumar, C.S.S.R. (2008). Microfluidic Synthesis of Nanomaterials. *Small, 4*(6), 698-711.

43. Sounart, T. L., Safier, P. A., Voigt, J. A., Hoyt, J., Tallant, D. R., Matzke, C. M., & Michalske, T. A. (2007). Spatially-resolved analysis of nanoparticle nucleation and growth in a microfluidic reactor. *Lab on a Chip, 7*(7), 908-915.

44. Takahashi, K., Hattori, A., Suzuki, I., Ichiki, T., & Yasuda, K. (2004). Non-destructive on-chip cell sorting system with real-time microscopic image processing. *Journal of Nanobiotechnology, 2*(1), 5.

45. Thompson, D. T. (2007). *"Using gold nanoparticles for catalysis."* Nano Today 2(4): 40-43.

46. Wang, Z., Zhang, J., Ekman, J. M., Kenis, P. J. A., & Lu, Y. (2010). DNA-Mediated Control of Metal Nanoparticle Shape: One-Pot Synthesis and Cellular Uptake of Highly Stable and Functional Gold Nanoflowers. *Nano Letters, 10*(5), 1886-1891.

47. Weibel, D. B., & Whitesides, G. M. (2006). Applications of microfluidics in chemical biology. *Current Opinion in Chemical Biology, 10*(6), 584-591.

48. Weng, X., Zhang, J., Wu, Z., Liu, Y., Wang, H., & Darr, J. A. (2011). Continuous syntheses of highly dispersed composite nanocatalysts via simultaneous co-precipitation in supercritical water. *Applied Catalysis B: Environmental, 103*(3–4), 453-461.

49. Winkler, K., Kaminska, A., Wojciechowski, T., Holyst, R., & Fialkowski, M. (2011). Gold Micro-Flowers: One-Step Fabrication of Efficient, Highly Reproducible Surface-Enhanced Raman Spectroscopy Platform. *Plasmonics, 6*(4), 697-704.

50. Ying, J. Y. (2006). Design and synthesis of nanostructured catalysts. *Chemical Engineering Science, 61*(5), 1540-1548.

51. Zinoveva, S., De Silva, R., D. Louis, R., Datta, P., S.S.R. Kumar, C., Goettert, J., & Hormes, J. (2007). The wet chemical synthesis of Co nanoparticles in a microreactor system: A time-resolved investigation by X-ray absorption spectroscopy. *Nuclear Instruments and Methods in Physics Research Section A: Accelerators, Spectrometers, Detectors and Associated Equipment, 582*(1), 239-241.

VITA

Chelliah V. Navin was born in Chennai, India. He graduated in May 2009 with a Bachelor of Technology in Biotechnology from Karunya University, Coimbatore. Upon graduation, Navin worked as a Project Associate in the Dept. of Biotechnology at Indian Institute of Technology, Madras until July 2010. Navin concluded his work at IIT Madras to pursue his Master's degree in Chemical Engineering at Illinois Institute of Technology, Chicago in August 2010. He later transferred to Louisiana State University, Baton Rouge in January 2011, where he will be awarded Master of Science by research in Biological and Agricultural Engineering in December 2012. Navin will continue his research further to pursue his Doctorate of Philosophy in Engineering Sciences with a major concentration in Biological Engineering at Louisiana State University, Baton Rouge. His technical interests include Bio-Energy, Bio-Chemical Engineering and Catalysis.